RL-TR-95-199
Final Technical Report
October 1995

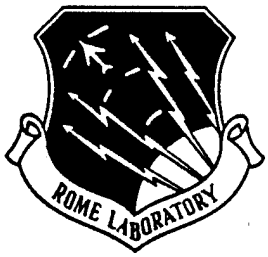

HIGH SPEED FREE SPACE DYNAMIC INTERCONNECTS FOR PHOTONIC RANDOM OPTICAL MEMORY ACCESS (PROMAC)

OptiComp Corporation

Peter S. Guilfoyle

Rome Laboratory
Air Force Materiel Command
Griffiss Air Force Base, New York

This report has been reviewed by the Rome Laboratory Public Affairs Office (PA) and is releasable to the National Technical Information Service (NTIS). At NTIS it will be releasable to the general public, including foreign nations.

RL-TR-95-199 has been reviewed and is approved for publication.

APPROVED: Bernard J. Clarke

BERNARD J. CLARKE, Captain, USAF
Project Engineer

FOR THE COMMANDER:

JOSEPH CAMERA
Technical Director
Intelligence & Reconnaissance Directorate

If your address has changed or if you wish to be removed from the Rome Laboratory mailing list, or if the addressee is no longer employed by your organization, please notify RL (IRAP) Griffiss AFB NY 13441. This will assist us in maintaining a current mailing list.

Do not return copies of this report unless contractual obligations or notices on a specific document require that it be returned.

REPORT DOCUMENTATION PAGE

Form Approved
OMB No. 0704-0188

1. AGENCY USE ONLY (Leave Blank)	2. REPORT DATE	3. REPORT TYPE AND DATES COVERED
	October 1995	Final ----

4. TITLE AND SUBTITLE
HIGH SPEED FREE SPACE DYNAMIC INTERCONNECTS FOR PHOTONIC RANDOM OPTICAL MEMORY ACCESS (PROMAC)

5. FUNDING NUMBERS
C - F30602-91-C-0125
PE - 62702F
PR - 4594
TA - I5
WU - J3

6. AUTHOR(S)
Peter S. Guilfoyle

7. PERFORMING ORGANIZATION NAME(S) AND ADDRESS(ES)
OptiComp Corporation
P.O. Box 10779
Zephyr Cove NV 89448

8. PERFORMING ORGANIZATION REPORT NUMBER
N/A

9. SPONSORING/MONITORING AGENCY NAME(S) AND ADDRESS(ES)
Rome Laboratory/IRAP
32 Hangar Rd
Griffiss AFB NY 13441-4114

10. SPONSORING/MONITORING AGENCY REPORT NUMBER
RL-TR-95-199

11. SUPPLEMENTARY NOTES
Rome Laboratory Project Engineer: Bernard J. Clarke, Captain, USAF/IRAP/ (315) 330-4581

12a. DISTRIBUTION/AVAILABILITY STATEMENT
Approved for public release; distribution unlimited.

12b. DISTRIBUTION CODE

13. ABSTRACT (Maximum 200 words)

High speed digital memory (ECL, GaAs) currently used in high performance computer technologies relies on expensive and power consumptive chips. These memories provide only marginal densities per chip (4-16K bit). However, through the integration of optical interconnects and volume storage technologies (coupled with alternative GaAs structures), an increase in speed as well as a decrease in power consumption can be realized. Thus, increased storage densities and faster access rates can be achieved. The laboratory prototype (a single wavelength, tunable laser diode with a diffraction grating) has demonstrated that random beam deflection in the nanosecond regime is possible using tunable laser diodes and a dispersive medium. PROMAC (Photonic Random Optical Memory Access) is a low inertia, low power, subnanosecond, parallel, angular scanning device that exploits free space optical interconnects. When PROMAC is combined with volume holographic memories in parallel structures, subnanosecond gigabyte random access memory storage configurations are possible. The final design integrates two device technologies, which include a multiple quantum well (MQW), distributed Bragg reflection (DBR), electronically tunable, laser diode array, and a waveguide hologram with a blazed grating and/or holographic grating.

14. SUBJECT TERMS
Optical memory, Tunable laser diode, Volume holographic optical interconnect element

15. NUMBER OF PAGES
72

16. PRICE CODE

17. SECURITY CLASSIFICATION OF REPORT	18. SECURITY CLASSIFICATION OF THIS PAGE	19. SECURITY CLASSIFICATION OF ABSTRACT	20. LIMITATION OF ABSTRACT
UNCLASSIFIED	UNCLASSIFIED	UNCLASSIFIED	UL

Table of Contents

List of Figures

List of Tables

HIGH SPEED FREE SPACE DYNAMIC INTERCONNECTS FOR PHOTONIC RANDOM OPTICAL MEMORY ACCESS (PROMAC)

1.0 Introduction

OptiComp Corporation is pleased to submit to Rome Laboratory, a final report titled, "High Speed Free Space Dynamic Interconnects for Photonic Random Optical Memory Access (PROMAC)". This 12 month research project was performed in response to the solicitation topic titled "Optical Memories" which was part of the Broad Area Announcement (BAA) #91-01-PKRL.

PROMAC (photonic random optical memory access) is a low inertia, low power, sub-nanosecond, parallel (eg. 64 bit wide), angular scanning device which exploits free space optical interconnects. When PROMAC is combined with volume holographic memories in parallel structures, subnanosecond gigabyte random access memory storage configurations are possible. The optical memory addressing system is highly competitive with respect to speed and power consumption when compared to conventional electronic implementations. The primary objectives of the PROMAC program are:

- To evaluate the feasibility of high speed, low power, random access, free space optical interconnect technology.
- To determine whether this architicture is applicable for massive, digital optical memory in optoelectronic computing devices.
- To demonstrate a single channel subsystem which will allow sub-nanosecond interconnects.

The final design integrated two device technologies which included a multiple quantum well (MQW) distributed Bragg reflection (DBR) electronically tunable laser diode array and a waveguide hologram with a blazed grating and/or holographic diffraction grating. The following parameters were observed in the overall architecture:

- High speed switching (~1 ns),
- High bandwidths in each channel (> 1 GHz),
- Low cross-talk and high signal-to-noise ratio (15 db/bit), and
- Low energy consumption (800 aJoules/switch interconnect)
- Large optical memory address field (> 10 MBytes)

High speed digital memory (ECL,GaAs) currently rely on power consumptive memory chips. These memories provide only marginal densities per chip (4-16Kbit). However, through the integration of optical interconnects and volume storage technologies, coupled with alternative GaAs structures, an increase in speed as well as a decrease in power consumption can be realized. Thus, increased storage densities and faster access rates can be achieved.

Within digital memory applications, laser scanners are used to either write information on a medium or to interrogate a medium. The PROMAC architecture addresses the issue of reading high volume optical mediums of digital information at nanosecond random access speeds. Thus, the I/O bottleneck problem is solved with raw speed. Current applications include: digital optoelectronic computing, parallel readout of optical disks, volume holographic memory readout and some of the more conventional applications such as robotic vision systems and inspection systems.

2.0 Technical Principles Underlying the PROMAC Design

The basic principle of PROMAC is demonstrated in Figures 1a & b. Scanning systems may be configured as angular deflection systems. Figure 1a depicts the use of an acousto-optic (AO) cell to perform angular deflection by the interaction of light and sound (the photon-phonon effect). This method is typically limited to microsecond-type scan rates due to the limited acoustic velocities of AO crystals. However, this method does rely on grating diffraction.

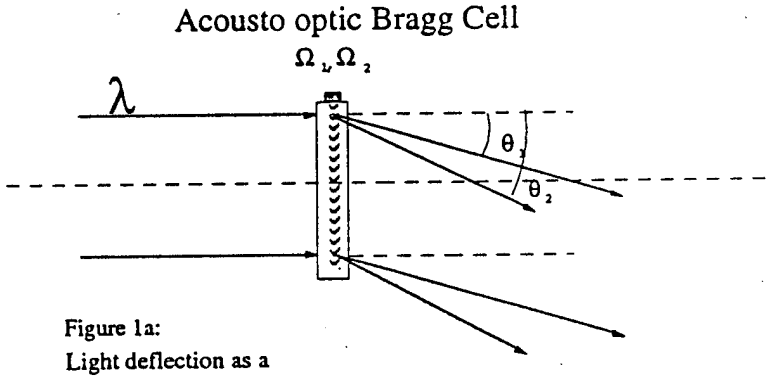

Figure 1a:
Light deflection as a function of Acousto optical frequency.

An alternative method is to fix a high resolution grating as shown in Figure 1b and to change the incoming wavelength. Changing the frequency of the acoustic grating alters the propagation direction of the light beam. By replacing the acousto-optic cell with a fixed diffraction grating, a change in wavelength also alters the propagation direction of the light beam [1]. An electronically tunable source mechanism or a DBR laser

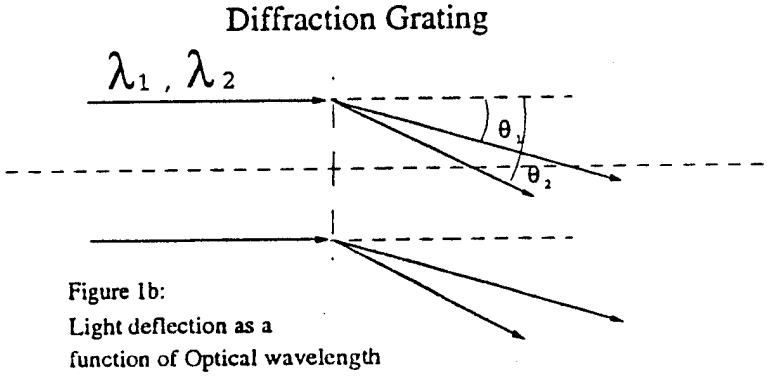

Figure 1b:
Light deflection as a function of Optical wavelength

capable was utilized to accomplish the program objectives. This laser was capable of randomly changing several angstroms (>100 Å) in wavelength in sub-nanosecond time periods. When this method is compared to the acousto-optic approach, far greater speeds may be obtained. Furthermore, monolithic integration is also possible. It is anticipated that this integrated approach of scanning will offer advantages in speed (spots/sec), spectral resolution ($\Delta l/l$), holographic separation ($\lambda_1-\lambda_2/\lambda$) [2 and 3], and scan efficiency (photon energy with respect to drive energy) [4].

Optical direction of propagation is a function of the period of the acoustic wave within the cell. Changing the frequency of the acoustic grating, alters the propagation direction of light beams. In semiconductor diode lasers, induced transitions occur between conduction and valence bands, but not between discrete energy levels. Therefore, the gain-bandwidth region is greater in semiconductor lasers than in gas or solid state lasers. High gain bandwidths permit a wide adjustment in the desired center frequency of the laser. To achieve lasing, the resonance condition for a single longitudinal mode must be obtained. Conventional MQW lasers routinely accomplish this objective. However, to change the wavelength, the second condition of cavity length adjustment must also be satisfied.

Electronically tuned bandwidths of 100-200 Å have been achieved to date. The bandwidth depends on factors such as the type of semiconductor compound used, the structure of the active region and the fabrication technology utilized. In order to change frequency, electrons are injected into the passive part of the laser (without inversion). Consequently, the density of electrons in the active region does not change. In addition, because the tuning electrons are not in the active region, the temporal intensity transitional process is unaffected. Only the phase of the emitted electro-magnetic wave is changed. Therefore, the process of wavelength tuning in a DBR laser is inherently a low inertia process. Wavelength switching times of ~nanoseconds or less can therefore be achieved. This switching speed becomes a function of second order drivers such as the size of electrodes (capacitive loading effects) and driver circuitry (VSWR effects).

3.0 Task Structure

The work plan for this contract consists of five primary tasks:

Task 1: Laboratory evaluation of a single channel PROMAC,

Task 2: MQW DBR wavelength tunable laser diode assessment,

Task 3: System architectural investigation,

Task 4: Chromatic dispersion analysis

Task 5: Final report.

3.1 Laboratory Evaluation of a Single Channel PROMAC

OptiComp has designed, fabricated and demonstrated a single wavelength, tunable laser diode with a diffraction grating coupled with a single channel Bragg cell. A primary objecrtive was to integrate a PROMAC prototype which would assist in evaluating the performance of the DBR laser through spatial and temporal mode characterization. The collimation, imaging and polarization optics used in the laboratory evaluation were developed under OptiComp's DOC II program with Rome Laboratory and SDIO in conjunction with ONR. When PROMAC is combined with volume holographic memories in parallel, structures (Figure 2), subnanosecond gigabyte random access memory storage congigurations are possible.

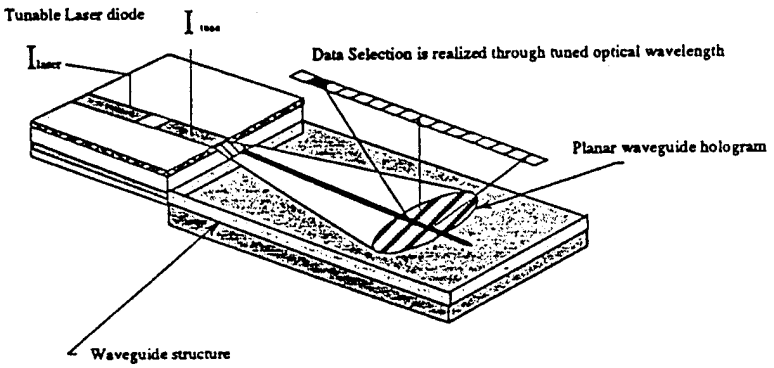

Figure 2: Single channel DBR laser integrated with a planar waveguide structure

3.1.1 Optical System Layout

Figure 3 demonstrates the optical system layout used in this evaluation. The DBR laser diode is driven by two channels of a LeCroy 9109 dual arbitrary waveform generator. Output radiation (~1.5 μm) from the tunable DBR laser source is transmitted into a high numerical aperture (NA: 0.65) laser collimator. The laser collimator is a six element system which is optimized for minimal phase distortion to the spatial wavefront ($\lambda/50$ rms). After collimation, the beam is directed onto a blazed grating where the zero order deflected beam is focused through a 100 mm plano convex lens onto a 200 μm fiber. This zero order output is then fed into a scanning optical spectrum analyzer. The first order deflected light is focused 700 mm beyond the diffraction grating slightly de-tuning the collimation lens to this focal length. A 200 mm cylinder lens vertically focuses the light (perpendicular to the diffraction angle) into a pair of 50 μm fiber core, 250 MHz (1.4 ns rise time), InGaAs PIN photodiode/transimpedance amplifiers. Each of the fiber pigtails are horizontally positioned to detect the diffracted beam for a particular DBR spectral mode hop (random mode transition). These amplifier outputs are recorded using an oscilloscope camera on a 350 MHz Tektronix-11302 scope to provide real time measurement of the instantaneous spectral output at selected modes with a 1 nsec resolution.

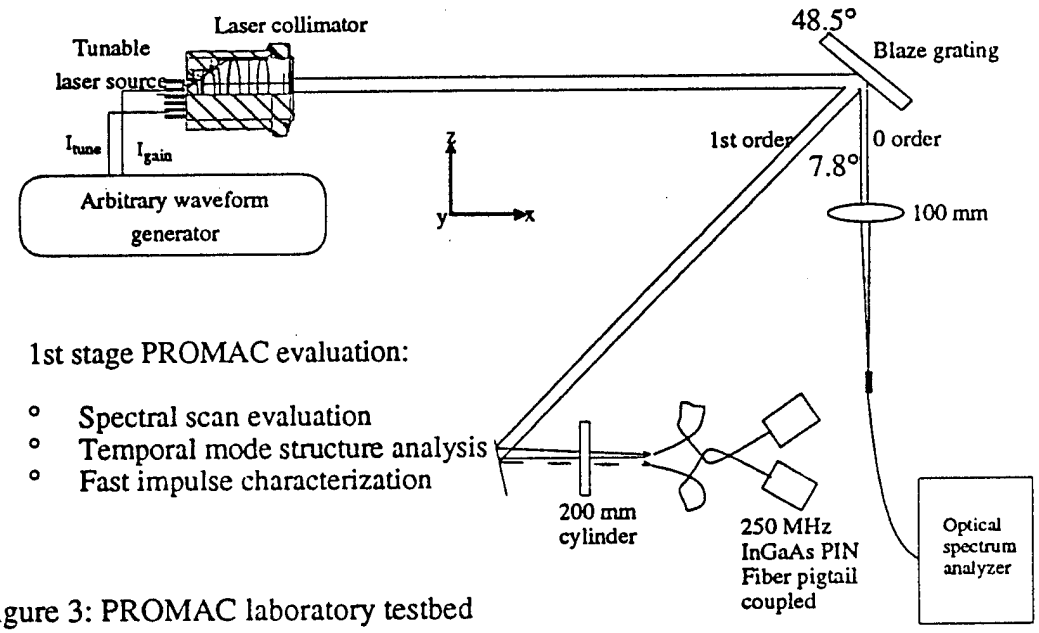

Figure 3: PROMAC laboratory testbed

3.1.2 DBR Laser Description

Figure 4 is a cross-section of an electronically tunable laser with an internal DBR grating region. Feedback is realized due to internal reflection from the grating. Bragg conditions can only be satisfied for single wavelengths. The laser is mounted P side up. The N side is mounted to a copper heat sink. This laser has three electrodes: 1.) gain current, 2.) tuning current and 3.) ground. The first electrode serves as a conventional gain input for amplification of the active region. Electrons are also injected into the grating region through the second electrode input.

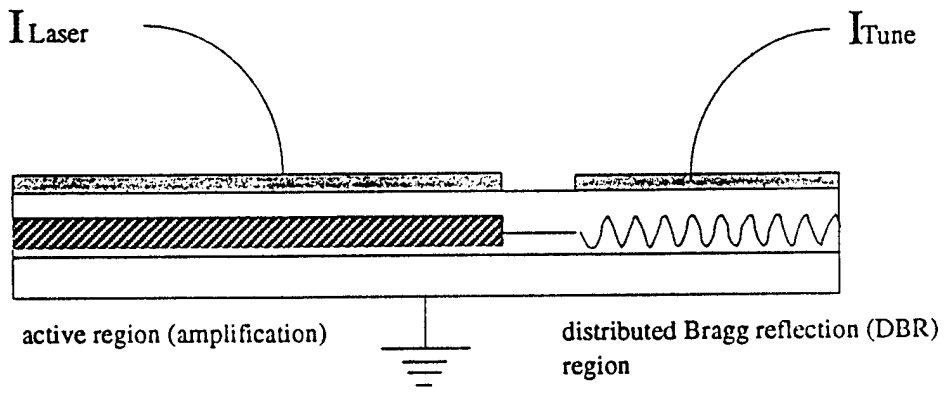

Figure 4: Longitudional structure of two section electronically tunable MQW distributed Bragg reflection lasers.

These electrons change the optical index of refraction within the grating region. This results in an effective grating spacing change which results in an optical resonance frequency shift. Any electrons that are accidentally injected into the passive region of the laser do not effect the active amplification region. Only the phase of the emitted electromagnetic wave is changed. Therefore, the process of wavelength tuning in the DBR laser is a low inertia process.

3.1.3 Grating Analysis

The diffraction grating utilized is described by the following Bragg diffraction equation shown in Figure 5. Differentiating angle β with respect to λ, is expressed by the following equation:

$$\frac{\delta B}{\delta \lambda} = \frac{m}{a*\cos(B)}$$

Using the above values, a chromatic angular dispersion of 0.003416 degrees / Å or 0.43 milliradians / 7.2 Å hop can be derived for the prototype system. Higher angular dispersions can be achieved by using either a finer grating, a second order diffraction beam, or by configuring the system for a larger diffraction angle. For the prototype, $\alpha = 48.5°$ and $\beta = 8.3°$ so that the reflected 0 order beam could be observed with the spectrum analyzer. Thus, the diffraction grating also functions as a beam splitter. A post-diffraction optical system path length of 700 mm provides a deflection of 0.31 mm/mode shift. The observed beam deflection is actually 3.61 mm for a 12 jump shift (87.5 Å) [5].

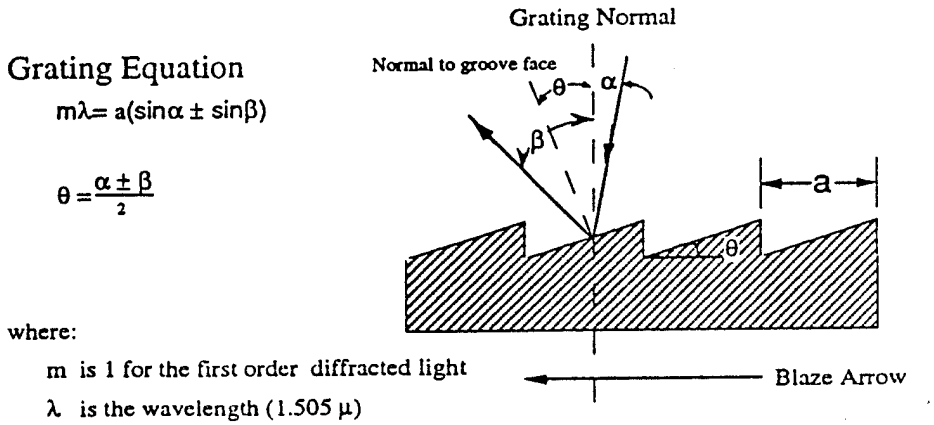

Figure 5: Cross-section of a blazed diffraction grating

Diffraction Grating Handbook
Staff of Milton Roy

3.1.4 Drive & Data Acquisition System Layout

An optical spectrum analyzer with a 0.8 angstrom resolution and a 350 MHz dual channel, real time oscilloscope was used to record the data. A GPIB data acquisition system was utilized to characterize the data sensing instrumentation. Electrical input into the DBR laser was generated by two channels of a 250 MHz, arbitrary waveform generator. Two independent, programmed waveforms were generated. The first waveform was a single value wave form to provide DC drive input to the gain region of the DBR laser. A variable amplitude stepped waveform was input into the tuning region of the laser. Each output channel of the arbitrary waveform generator was followed by a 50 ohm power splitter for monitoring on a 100 MHz oscilloscope. The output from each splitter then fed a 100 ohm series resistance to each electrode for the DBR spectral mode measurements and a 50 ohm series resistance for the high speed mode hopping experiments.

3.1.5 Test Results of the PROMAC Laboratory Experiment

The following objectives were met through the integration of a single element DBR laser diode with an external blazed grating and fiber coupled PIN photodiodes:

1) Establish the spectral mode structure of the DBR laser.
2) Characterize the fast impulse response of the system.
3) Parameterize the system resolution.

Spectral scan results

A variable voltage stepped waveform was produced from the arbitrary waveform

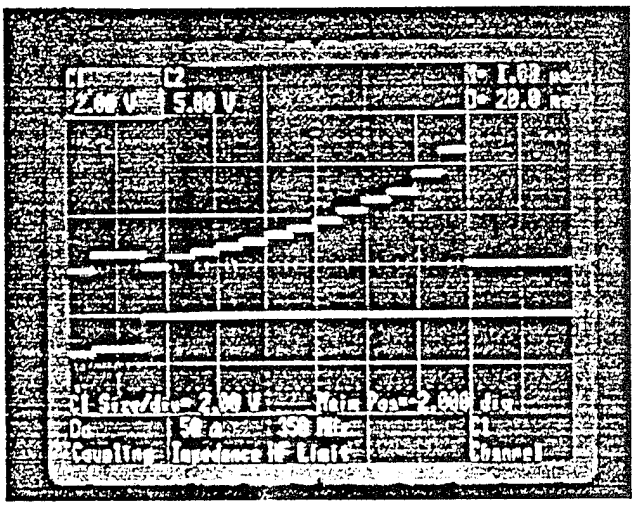

Figure 6: Top trace- input waveform into DBR tuning region
Bottom trace - input waveform to the gain region of the laser

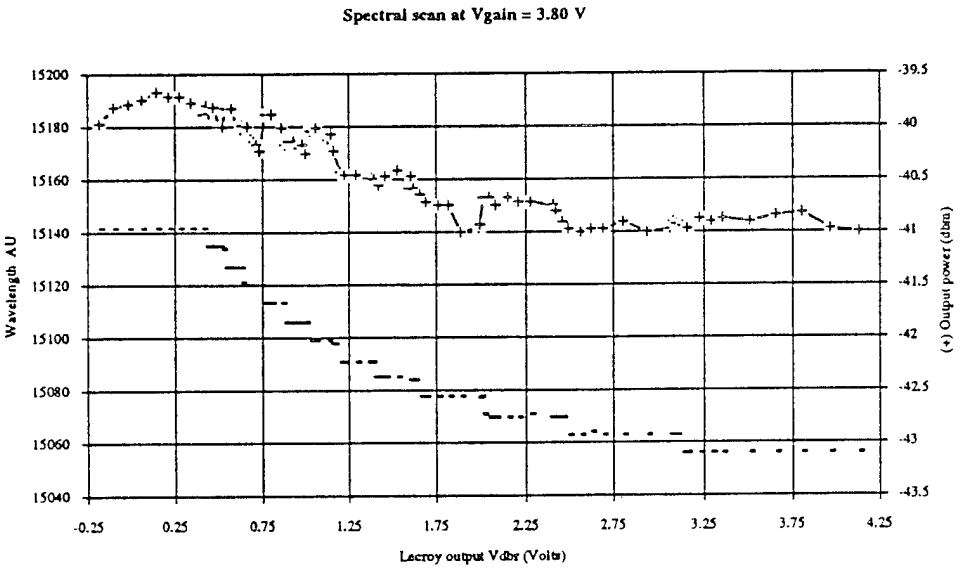

Figure 7: Graph of spectral results

generator (Figure 6). This waveform was calibrated to match the DC mode hop characteristics as measured and shown in Figure 7. The waveform was injected into the tuning region of the DBR laser diode through a 100 ohm resistance. The conditioned spectral output was then focused into a fiber which fed the optical spectrum analyzer. An equivalent circuit of the specified drive voltage connected through a 100 ohm resistor to the VDBR probe yields a measured relationship between spectral shifts, drive voltage and current (Table 1).

Table 1: Relationship between spectral shifts, drive voltage and current

Mode	VDBR	Current (ma)
0	0.20	1.72
1	0.48	1.26
2	0.60	0.67
3	0.70	0.21
4	0.81	1.22
5	0.95	2.6
6	1.07	4.11
7	1.26	5.86
8	1.48	8.21
9	1.75	10.76
10	2.12	12.00
11	2.64	16.46
12	3.20	26.00
13	3.65	30.00

Mode structure of the DBR laser

Figure 8 shows the DC characterization of the superposition of single mode performance of the DBR laser. Modes are spaced approximately 7 angstroms apart. This superposition depicts 13 modes, although two in the center and one at the end are not shown. Spectral widths measured were typically 1.6 angstroms at 10 db down, and were at close to the spectrum analyzer resolution limit.

Fast impulse characterization results

The spectral and temporal beam characteristics were measured for several constant values of current drive (I) with stepped values of I_{DBR}. With I_{DBR} alternating between modes 1 and 13 (12 "hops"), the spectral energy in the modes between the end modes during the hop was approximately 20 db below peak mode power. The scope traces shown in Figures 9a and 9b show the observed waveform from two detectors positioned at the starting and destination modes, when hopping back and forth between 10 and 30 MHz. Waveform degradation occurs beyond 30 MHz which is apparently due to the impedance mismatches at the die probe interconnect. The source waveform used in this experiment had a rise and fall time below 4 nsec.

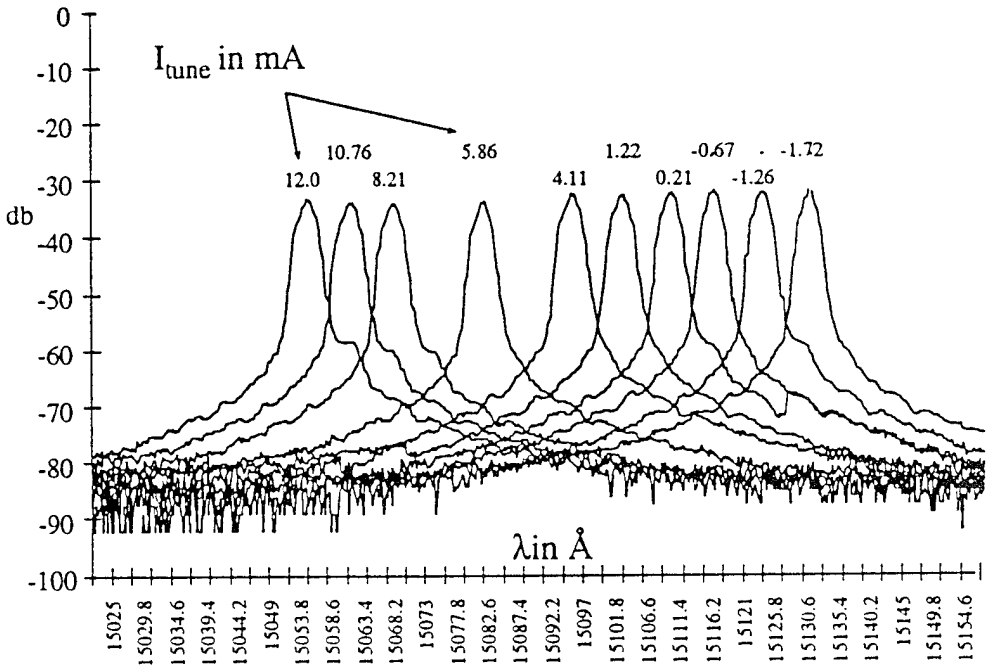

Figure 8: Superposition of discrete spectra of a tunable DBR laser from the optical spectrum analyzer

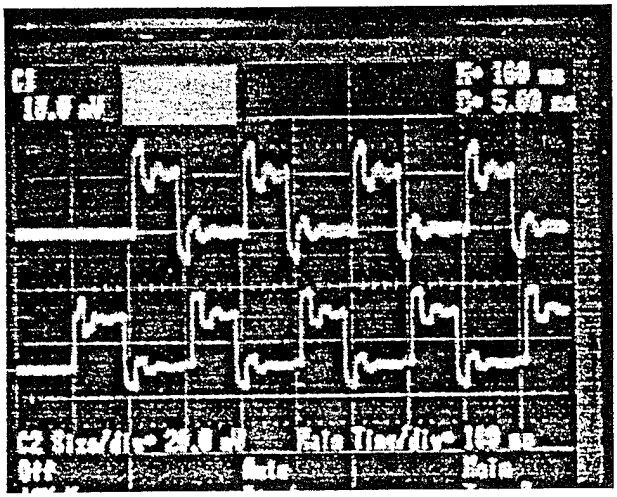

Figure 9a: 10 MHz scan rate

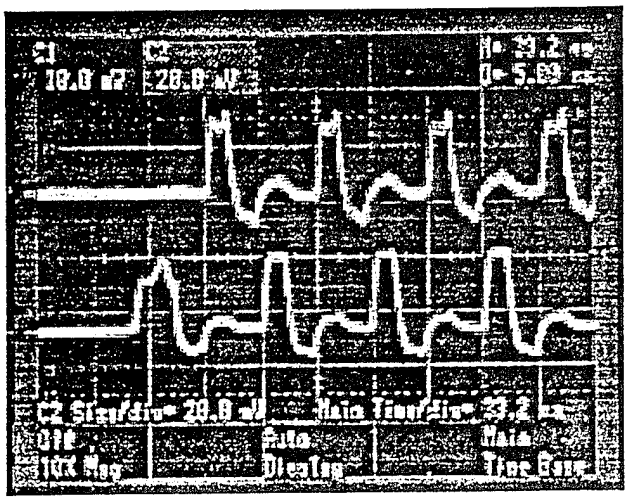

Figure 9b: 30 MHz scan rate

OptiComp performed a comprehensive architectural investigation. A summary of the most pertinent technical references is found in the Appendix. A final MQW DBR wavelength tunable laser diode design was generated in conjunction with David Sarnoff Reseach Center. The specifications for this design include:

1. A tuning range sufficient to obtain up to 64 selectable wavelengths (for each array element)
2. A wavelength which ranges between 0.8 -1.0 μm.
3. Up to 32 monolithic laser elements, each capable of 64 "spots"
3. A switching time < 1-10 ns
4. Single wavelength and single spatial mode with line width commensurate with 1.
5. A <1 μm astigmatism
6. Collinear, non-steering array output
7. A 50-250 μm center to center array spacing
8. Negligible cross-talk
9. Near field ≈ 1 x 4 μm
10. Mutual incoherence among collinear array lasers
11. High spatial and temporal coherence
12. Differential quantum efficiency of >30 percent
13. Power > 10 mW per element

3.2 MQW DBR Wavelength Tunable Laser Diode Assessment

3.2.1 Required Trade-offs to Achieve Tuning Goals Based on a Multi-Section DBR Laser

In order to achieve a large number of resolvable spots, the ratio of wavelength separation between adjacent "spots", $\Delta\lambda$, to line width, δl or δn, must be large. The line width measured in frequency, δn, is directly proportional to the line width measured in wavelength, $\delta\lambda$. If the derivative of $\lambda = \frac{c}{\nu}$

$$\text{then, } \delta\lambda = -\frac{c}{\nu^2}\delta\nu = -\frac{\lambda^2}{c}\delta\nu \qquad (1)$$

The objective of this program is to switch from one spot to another. Thus, continuous wavelength tuning is not required. It is actually more desirable to go discontinuously between wavelengths. Discontinuous jumping between wavelengths is characteristic of multiple section DBR tunable lasers in which no phase section tuning is included. A schematic of this device is shown in Figure 10.

Changing the refractive index of the Bragg grating section by injecting current, I_B, while maintaining a constant gain section current value, I_g, will tune the resonant reflecting wavelength

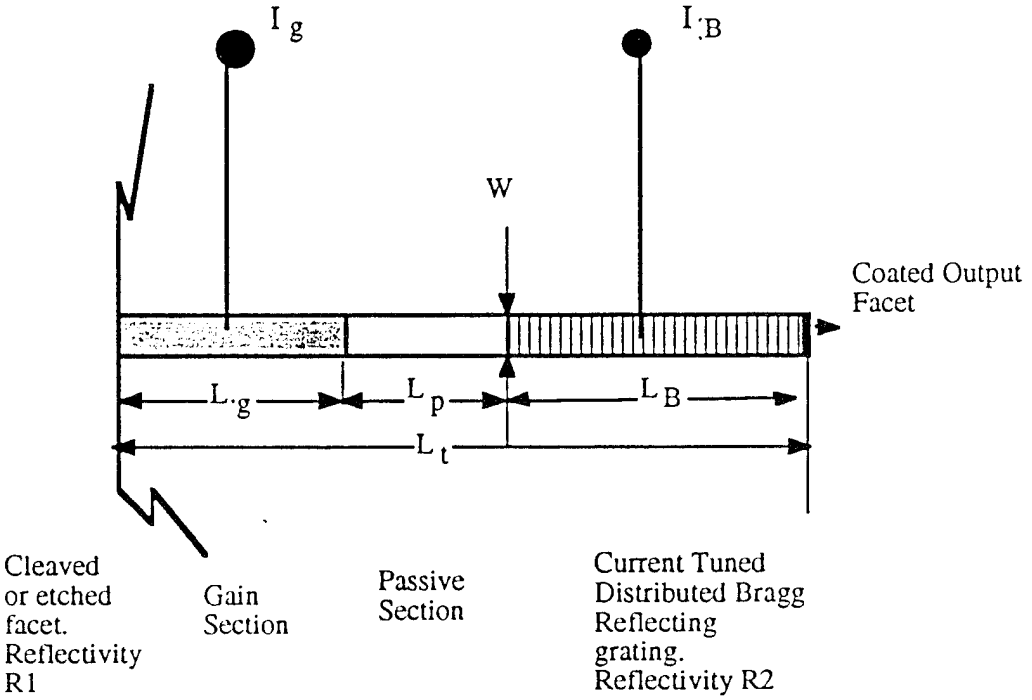

Figure 10: Schematic of a tuned DBR diode laser with a gain section, a passive section, and a current tuned Bragg reflecting section

of the Bragg grating and change the total phase length of the laser cavity. The phase length change results in a relatively small tuning of the wavelength of operation within one Fabry Perot (fp) mode of the cavity. This continues until the change in Bragg reflectivity is sufficient for the operation to (discontinuously) switch to the next fp mode. The fp modes are defined identically to those for a cleaved diode laser, except that the cavity length is taken as the length of the gain and passive sections plus the effective length of the Bragg grating. The wavelength spacing of the fp modes, $\Delta\lambda$, is given by [6]:

$$\Delta\lambda = \frac{\lambda^2}{2(n_g L_g + n_p L_p + n_B L_e)} \tag{2a}$$

For our initial estimates, the effective (group) refractive indicies of the three regions, n_g, n_p and n_B will all be equal to a single refractive index n_e. Thus,

$$\Delta\lambda = \frac{\lambda^2}{2n_e(L_g + L_p + L_e)} \tag{2b}$$

L_g and L_p are the lengths of the gain and passive sections respectively, and L_e is the effective length of the grating section which is defined as:

$$L_e = \frac{\text{Tanh } \kappa L_B}{2\kappa} \tag{3}$$

L_B is the length of the grating and κ is the grating coupling coefficient. The linewidth of Bragg reflecting diode lasers has been found to vary with cavity length as:

$$\delta_\nu = \alpha_\nu \left(\frac{n_g L_g}{n_g L_g + n_p L_p + n_B L_e} \right)^2 \tag{4a}$$

Approximating, by using a single refractive index,

$$\delta_\nu = \alpha_\nu \left(\frac{L_g}{L_g + L_p + L_e} \right)^2 \tag{4b}$$

and applying Equation (1) we obtain:

$$\delta\lambda = \alpha_\lambda \left(\frac{L_g}{L_g + L_p + L_e} \right)^2 \tag{5}$$

where:

$$\alpha_\lambda = -\frac{\lambda^2}{c}\alpha_\nu$$

Over the percentage range of tuning, we approximate α_λ as a constant.

A measured value of linewidth is used to find the value of α_λ. For a device with $L_p = 100\ \mu m$, $L_e = 50\ \mu m$ and $L_g = 400\ \mu m$, a line width of 1 MHz (10^6 Hz) is reported [6] which gives $\alpha_\lambda = 6.3 \times 10^{-9}\ \mu m$. To see the effect of varying the initial line width, we may make this more general by approximating:

$$\alpha_\lambda \approx 6.3 \times 10^{-9}\frac{\delta\nu}{10^6}\mu m \tag{6}$$

Using Equations (2b), (5), and (6) the desired ratio is:

$$\frac{\Delta\lambda}{\delta\lambda} = 7.94 \times 10^{13}\frac{\lambda^2}{n_e\delta\nu}\left(\frac{L_g + L_p + L_e}{L_g^2}\right) \tag{7}$$

An additional objective is to determine how much current and how much power is required for the independent tuning of the power requirements for operating the laser. The refractive index change produced in a grating region by current injection must be considered. It is assumed that the grating region has a simple heterostructure-junction active region at a bandgap which is higher than the operating wavelength. In this case, the index is not pinned by any induced emission-recombination.

The change of index with current has been described by several authors (see Appendix). Average values were used from References 7 and 8. For GaAs type materials, the change in index, δn, due to injecting a (change in) current ΔI (measured in mA) is well approximated by:

$$\delta n \approx 1.067\ \Delta I\ (mA)/\Gamma LW \tag{8}$$

where L is the length and W the width of the injection region measured in micrometers (μm). Γ is the usual confinement factor. For a Bragg reflecting grating operating on a guided mode, the change $\Delta\lambda$ in resonant wavelength λ is:

$$\Delta\lambda = \lambda\ \delta n/n_e \tag{9}$$

Under the same assumptions used to obtain Equation (2b), and using Equations (2b), (8), and (9), it follows that the required change in current to switch over a wavelength interval equal to the separation of adjacent fp modes is:

$$\Delta I(\text{in mA}) = \frac{\lambda W L_B}{2.14\Gamma(L_g + L_p + L_e)} \text{ (all lengths in } \mu\text{m).} \qquad (10)$$

Plots of ΔI, $\Delta\lambda/\delta\lambda$ and $\Delta\lambda$ against total cavity length L_t are given in Table 2 as well as Figures 11 and 12 . These figures were generated on an EXCEL spread sheet program which allows changes in the parameters. The parameter values are labeled in column A and the values are inserted in column B (in the same row as the labels). The program automatically generates the figures corresponding to the inserted values. Increasing the cavity length, results in improved resolution and decreased current requirements (Figures 11 and 12). There are, however, a number of restraints on the cavity length due to losses, grating efficiency and power requirements.

3.2.2 Wavelength Tuning Methods

The "conventional" tunable-multisection DBR (or distributed feed back) laser has been summarized by Hammer and others [9,10 and 11]. It is convenient to refer to this method as a Tunable Bragg Reflector (TBR) laser. A number of other approaches have also been considered. The current assessment indicates that the program objectives will be accomplished by a multi-section TBR which uses the sampled gratings described in Section 3.2.6 (Sampled Gratings).

Table 2: Values assumed for calculation of $\Delta\lambda$, $\delta\lambda$ and ΔI

A	B
L_g	500
L_p (init.val)	0
L_e	150
w	4
n_e	3.4
λ	1
Γ	0.1
L_p step	200
$L_B=2L_e$	300
dn	8.00E+06

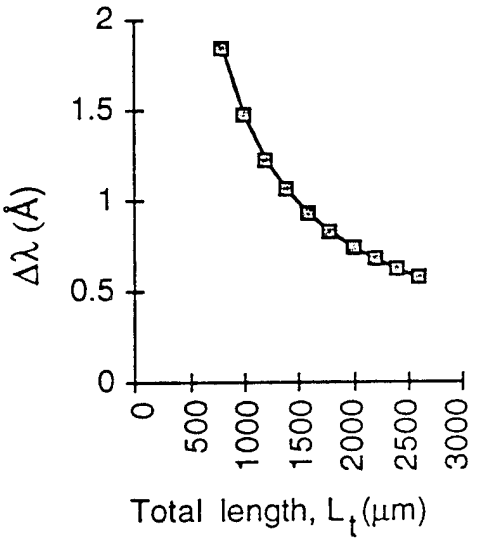

Figure 11: Plot of $\Delta\lambda$ vs total cavity length for the parameters shown in Table 2

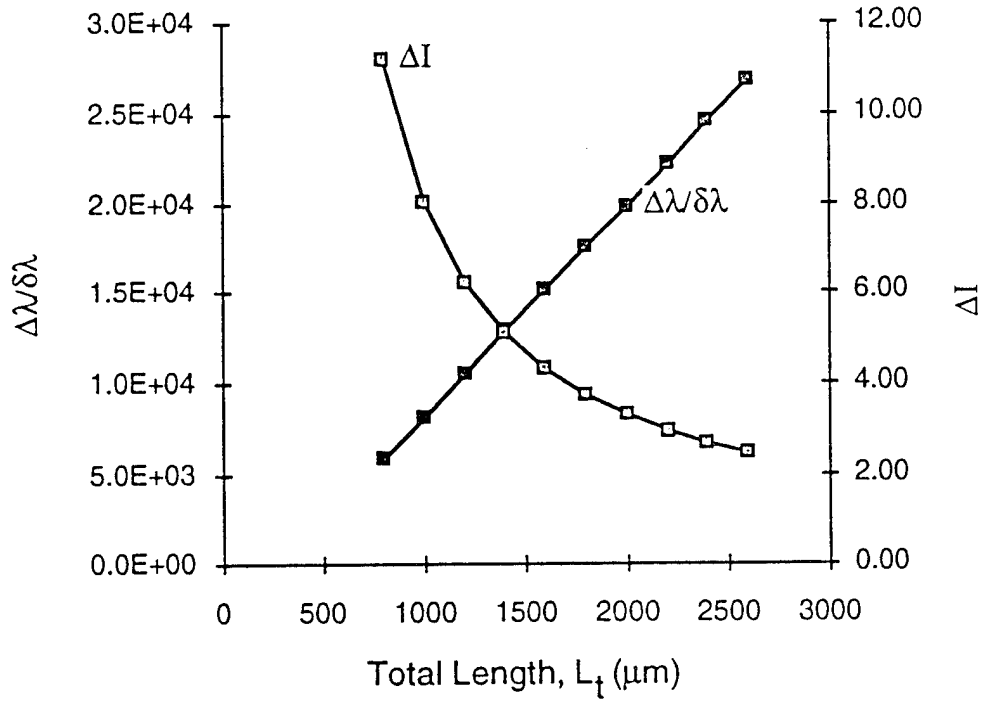

Figure 12: Plot of $\Delta\lambda/\delta\lambda$ and ΔI vs total cavity length for values tabulated in Table 2

3.2.3 Tunable-Multisection DBR TBR (Or Distributed Feed Back (DFB)) Laser

A schematic of a TBR diode laser is illustrated in Figure 13. The DBR grating can be described as a backward coupled filter that reflects light only over a narrow resonant wavelength range, which depends on the grating period and the effective refractive index in the grating region. The reflected wavelength is tuned by varying the injected current into the grating region which changes the effective refractive index. A phase section may be included to achieve continuous tuning. The advantages of this approach are summarized in Table 3.

Table 3: Comparison of diode-laser-wavelength-tuning methods

Approach	Tuning Range	Resolution (Tuning Range /Linewidth)	Advantage	Disadvantage
Multisection Tunable DBR (TBR)	100Å	High $\approx 10^4$	Continuous or discrete tuning. Familiar technology.	Multi-electrode tuning. High tuning power.
TBR with sampled gratings	570Å	To be determined, probably very high $\geq 10^4$	Continuous or discrete tuning. Low tuning power.	Multi-electrode tuning requires fine control.
Tunable Twin Guide (TTG)	100Å	High	Continuous- single-electrode tuning	Difficult growth, processing. High tuning power
Tunable Codirectional Filter (TCF)	570Å	High	Continuous-single-electrode tuning. Low tuning power.	Difficult growth and processing
VCSEL DBR	Possibly >100Å	High	Easy arrays, single control current	Thermal tuning
QW gain lever may be used to decrease tuning power in some methods.				

3.2.4 Tunable Twin-Guide (TTG) Laser

The grating using the TTG laser approach documented in references [12-15] is arranged in a plane parallel to the gain (active) region (Figure 13). The TTG laser is a actually a variation of a DFB laser. The grating typically has the same length as the gain region. The grating and gain regions are electrically isolated from, but optically coupled to each other. Thus, the grating can provide distributed optical feedback.

In Figure 13, E(x) is the optical mode of the composite waveguide formed by the two high index InGaAsP quaternary regions of this example. The n-InP contact and electrical isolation layer are sufficiently thin to allow the waveguide to operate in a single mode which links the grating and gain layers. AlGaAs materials can be used in an analogous way. Gain current (I_g)

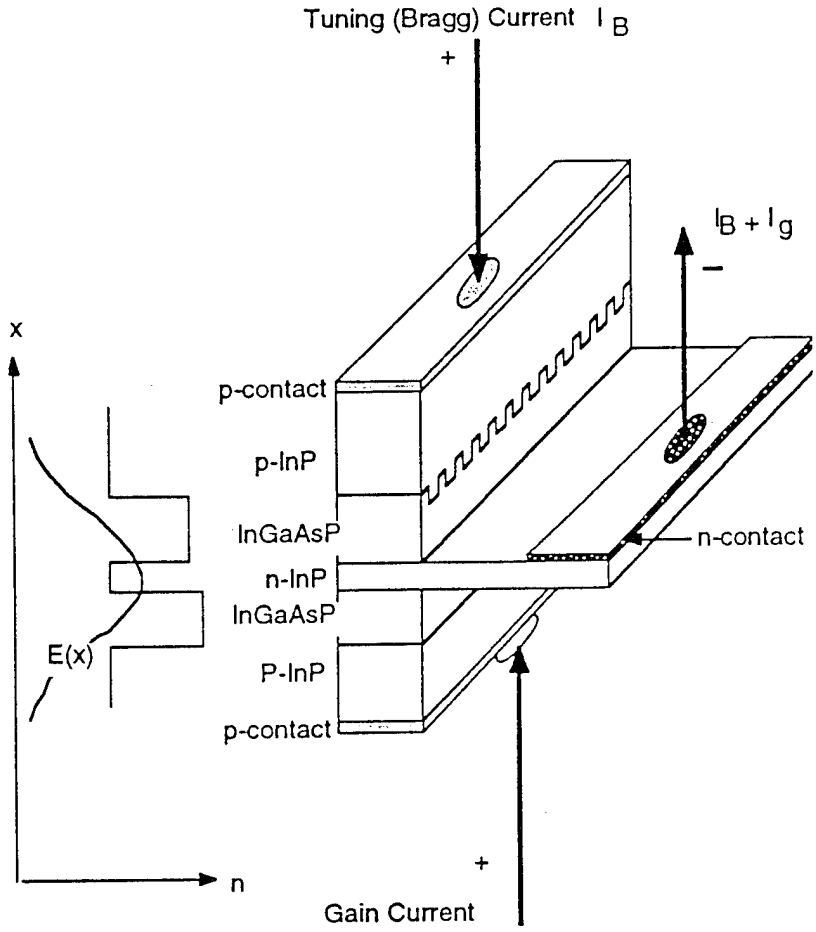

Figure 13: Tunable twin guide laser

injected through the lower p-contact controls the gain without affecting (to first order) the resonant wavelength of the grating. Tuning current (I_B) injected through the upper p-contact controls the resonant wavelength of the grating without (to first order) affecting the gain.

The advantages of this design as compared to the "conventional" TBR laser is that the grating shares the same physical length and waveguide mode of the active region which allows for continuous tuning by a single electrode. Additionally, as compared to "conventional" tunable DFB lasers, in which the grating also shares the physical length and waveguide mode of the active region, the tuning range is not limited by gain clamping because the grating is electrically isolated from the active region.

Continuous tuning occurs because the resonant grating wavelength and the DFB phase oscillation condition ("Fabry Perot" mode) are simultaneously tuned by the same amount as the

effective index of the guided mode is varied. This tuning may be described by the following equation. The resonant Bragg reflecting wavelength, λ_B, is given by:

$$\lambda_B = \frac{m\Lambda}{2n_e} \tag{11}$$

where Λ is the grating period , n_e the effective index and m the Bragg grating order.

The laser mode (wavelength mode) associated with this wavelength will have an integral number of guide wavelengths N_{fp} such that:

$$N_{fp} = \frac{2Ln_e}{\lambda_B} \tag{12}$$

where L is the cavity length or the effective length of the Bragg grating. Eliminating λ_B between these two relations we obtain:

$$N_{fp} = \frac{mL}{\Lambda} \tag{13}$$

This equation demonstrates that the order of the lasing wavelength mode is independent of the effective index for the TTG laser; and thus, continuous tuning within one wavelength ("Fabry Perot") mode is allowed. As the resonant Bragg wavelength is tuned, the phase length of the cavity is also tuned such that the number of wavelengths in the cavity, as measured in peak Bragg reflecting wavelengths, is constant.

In the conventional multisection TBR laser, the relationship corresponding to Equation (13) is:

$$N_{fp} = \frac{m(n_g/n_B L_g + L_B + n_p/n_B L_p)}{\Lambda} \tag{14}$$

Equation (14) shows that as the effective index in the Bragg section (n_B) is changed, the number of wavelengths in the cavity changes. This change can be compensated by varying the index of the phase section n_p. L_g, L_B, and L_p are the lengths of the gain, Bragg and phase sections respectively; n_g is the index of the gain section.

The most successful tuning results reported for a TTG laser [12] was 71 Å at 1.55 μm, at an output power of ≈ 1 mW. This approach has been extensively pursued at Siemens, although some work has been done in Japan. [11] The primary problem lies in growing a rather complex structure which requires a transverse n-contact sandwiched between two separate p-growths (This problem is similar to the TJS type of laser). The reported results to date are not impressive.

3.2.5a Tunable Codirectional Filter (TCF) Laser

Tunable codirectional filters have been discussed at length by a number of authors [16-21]. Tunable diode lasers using such filters have been reported by Chuang and Coldren [20], Chuang et al[22], and by Illek et al [23].

A TCF laser is illustrated schematically in Figure 14. The upper waveguide, the grating (or Bragg) waveguide in this arrangement, is formed by the p-waveguide layer sandwiched between the upper p-clad and the n layer. A grating with period Λ is formed in the tuning region of the upper waveguide. A lower waveguide is formed by gain layers sandwiched between the n region and the lower p-clad. The gain layers consist of separate confinement heterostructures and a quantum well (or wells) SCH-QW. The tuning (grating) waveguide mode has an effective index n_t and the gain wave guide mode has an effective index n_g. The modes have an evanescent overlap. The grating provides strong coupling between the mismatched waveguides at a reso-

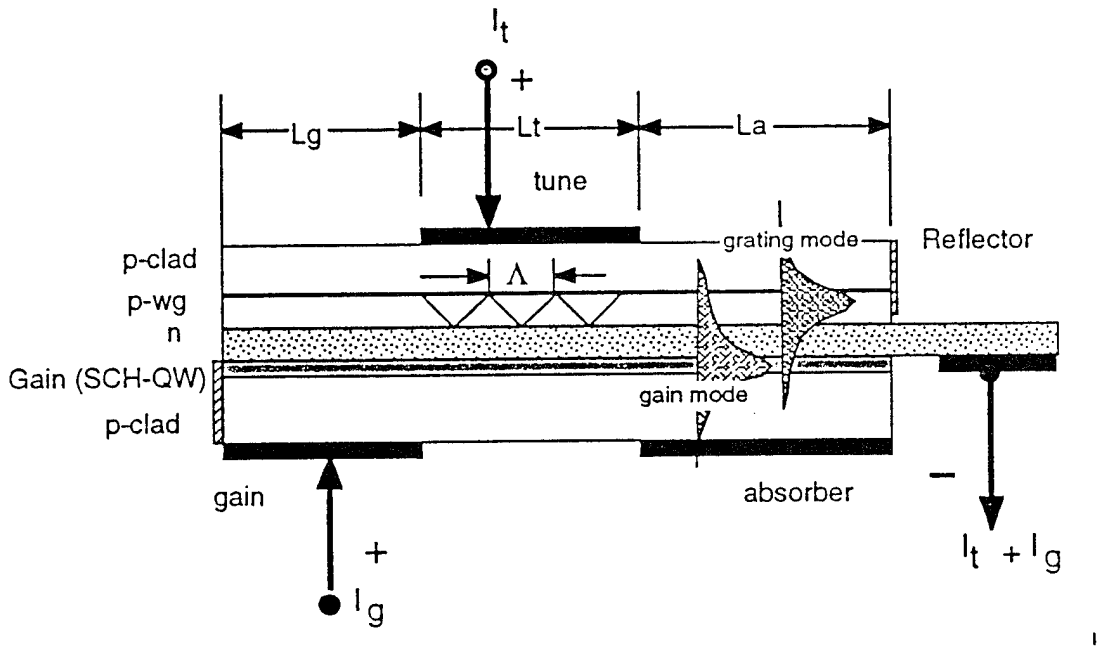

Figure 14: Tunable codirectional filter (TCF) laser

nance wavelength λ_t, which is given by:

$$\lambda_t = \Lambda\ (n_g - n_t) = \quad \Lambda\Delta n \tag{15}$$

The waveguides are substantially uncoupled off resonance because of the index difference.

Off resonance lasing is avoided by the absorption of the gain waveguide outside of the region where current is injected. Only light coupled to the grating guide, reflected by the right mirror of the grating guide (Figure 14), and recoupled back into the gain guide will have low loss, and thus permit oscillation.

The index of the grating region is tuned by varying the injection current to that region. The grating region is electrically isolated from the gain region in a manner that is analogous to that used in the TTG laser described above. When n_t is changed by δn_t, the resonance wavelength change is given by:

$$\frac{\Delta\lambda_t}{\lambda_t} = \frac{\delta n_t}{\Delta n} \tag{16}$$

In the "conventional" TBR laser, where the grating acts as a contra-directional filter, the corresponding relation is:

$$\Delta\lambda_B,\lambda_B\ ) = \frac{\delta n_B}{n_e} \tag{17}$$

where n_e is the average effective index of the guides. Thus, the TCF laser tuning is increased compared to the TBR laser tuning by the ratio of the effective index divided by the difference of the index between the evanescently coupled guides.

In the TCF structure described by Chuang et al [22] which uses a strained layer quantum well and operates at $\approx 0.97\ \mu m$, a Δn of 0.124 can be calculated (using MODEIG) with $n_e \approx 3.31$ to give approximately a thirty fold increase in tuning range, as compared to using similar materials and structures in a TBR laser.

There is, however, a caveat with the TCF laser. As shown below, the ratio of coupling linewidth dlt to the separation of fp modes $\Delta\lambda$fp is large so that the coupling grating does not ensure single wavelength mode operation. This important defect has not yet been addressed in the literature. The ratio of tuning bandwidth to fp mode spacing can be calculated using the

estimated tuning bandwidth of a codirectional filter given by Griffel and Yariv. [18] When this is done, the following ratio is expected:

$$\delta\lambda_t,\Delta\lambda_{fp}) \approx \frac{1.6(L_g + L_t + L_a)}{L_t} \frac{n_e}{\Delta n} \frac{1}{\left(1 - \frac{1}{\Delta n}\frac{d\Delta n}{d\lambda}\right)} \qquad (18)$$

The slope $\frac{d\Delta n}{d\lambda}$ was calculated for the structure cited above [23] to be 0.25/μm. Using this value and the other values [23], we obtain:

$$\frac{\delta\lambda_t}{\Delta\lambda_{fp}} \approx \frac{44.2(L_g + L_t + L_a)}{L_t} \qquad (19)$$

Because the total length ($L_g + L_t + L_a$) must be greater than or equal to the tuning length L_t, the tuning bandwidth will be at least 44.2 times as large as the fp spacing. It is clear that the tuning bandwidth will be greater than the fp bandwidth for all practical cases.

It should be noted that the spectrometer plot in Illek et al [23] which shows single mode operation has a resolution of > 2 Å, but still shows some structure in the main line. This clearly indicates that Illek et al [23] are not observing single wavelength mode operation.

3.2.5b VCSEL

Vertical cavity surface emitting lasers (VCSEL). VCSELs have the advantage of being easily manufactured into densely packed 2-dimensional arrays [23a]. VCSEL technology however is relatively immature, and work on tunable VCSELs is even more preliminary. To date, about 20 Å of tuning has been demonstrated by workers at Universität Ulm [23b], using resistive heating of one of the Bragg mirrors. Recent work at UC Santa Barbara has demonstrated VCSEL operation of >100 °C [23c], which could be exploited in tunable VCSELs with >100Å tuning range. Though the tuning mechanism is thermal, the relatively low thermal mass and impedance of VCSEL lasers may still allow high speed operation, though probably not as fast as carrier injection in in-plane lasers. The tuning is also limited to $\Delta\lambda/\lambda \leq \Delta n/n$, as in a conventional TBR laser.

3.2.6 Sampled Gratings

Jayaraman, Cohen and Coldren [24] and Jayaraman, Mather, Coldren and Dapkus [24a] have demonstrated very broad band tuning (293 Å) of a TBR laser using a pair of gratings containing a long intensity periodicity to act in a manner similar to a comb filter (Figure 15).

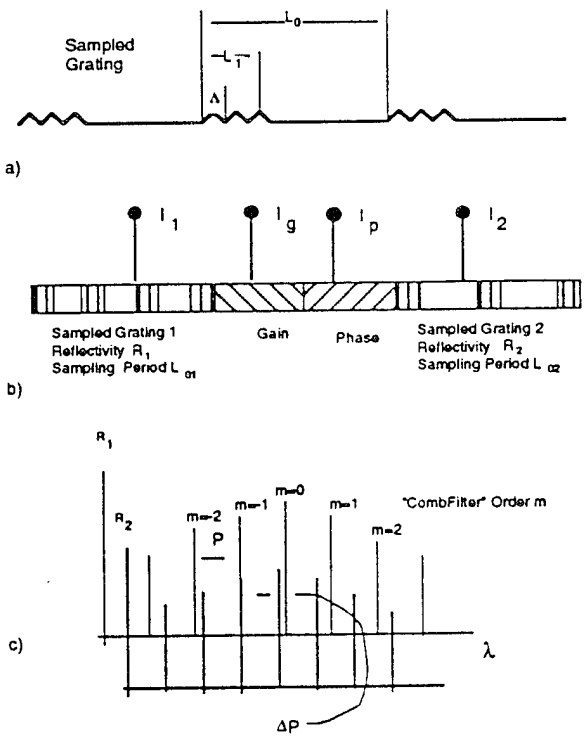

Figure 15 a) Schematic of a sampled grating - Λ is chosen to reflect the desired center λ.
b) Schematic of a TBR laser using current tuned sampled gratings on each end.
c) Representation of reflectivity of sampled gratings as a function of wavelength. The sampling period L_0 results in a "comb filter response.

Figure 15a shows a schematic of a sampled grating where Λ is chosen to reflect the desired center wavelength. Figure 15b is a schematic of a TBR laser using current tuned sampled gratings on each end. Sampled grating 1 has a sampling period different than that of sampled grating two. Figure 15c is the sampling period; L_0 results in a "comb filter" response with a comb interval P. The difference in the comb interval between grating 1 and grating 2 is ΔP. If one of the gratings is tuned with injection current, lasing would occur where a "finger" of R_1 overlaps a finger of R_2. If the refractive index tuning range of one of the gratings is $\Delta n/n$, the tuning range for this device is:

$$\frac{\Delta\lambda}{\lambda} = \frac{\Delta n}{n}\frac{P}{\Delta P} \qquad (20)$$

When compared to a TBR with unsampled gratings, an increase in tuning range is realized by the ratio $P/\Delta P$. In the work by Jayaraman et al [24a], P_1 was 59 Å (L_{01} = 50μm) and P_2 was 66Å (L_{02} = 50 μm) at an operating wavelength around 1.47 μm. Thus, the increase in tuning range over an unsampled grating is ≈ 10. Recent analysis suggests >1000Å is possible in optimized devices at 1.55 μm.

3.2.7 Quantum Well Gain Lever Approaches

The quantum well gain lever can be used in a number of the approaches previously described to obtain an increased refractive index change as compared to simple carrier injection in a lasing region. A description of the gain lever was published by Vahala, Newkirk and Chen in 1989 [25]. Subsequent work was reported by Lau and others [26-30].

Figure 16a is a schematic of a quantum-well gain-lever semiconductor laser. The short region is called the control, and the large region the slave. Figure 16b is a plot of gain versus carrier density for a single quantum well laser. Note the gain saturation at high injected carrier densities which is typical for quantum well operation.

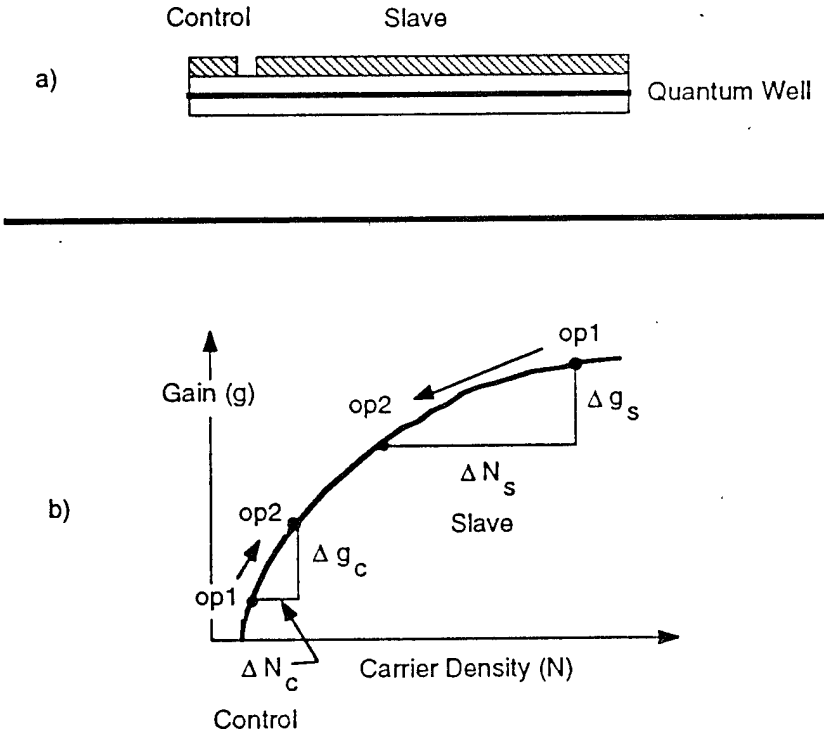

Figure 16 a) Schematic of quantum-well gain-lever semiconductor laser
(short region - control; large region - the slave)
b) Plot of gain versus carrier density for a single quantum well laser

Assume that the injected current in the slave region is held constant at the operating point, op1. If the injected carriers of the control region are changed from the operating point op1 to the operating point op2 (carrier density in control region is increased by ΔN), then the gain in the control region increases by Δg_c. Because of gain clamping, the gain in the slave region must decrease by the same amount. Thus, $\Delta g_s = -\Delta g_c$. Consequently, the carrier density in the slave

region decreases by ΔN_s which is larger than ΔN_c because of the sublinear (saturated) characteristic of the gain-carrier density relation for quantum well lasers. This effect is called the gain lever and allows a large change in carrier density to be obtained in the slave region with a relatively small change of injection carriers in the control region. The refractive index change is directly proportional to the carrier density change. Thus, the gain lever can be use to obtain relatively large intracavity refractive index changes for use in FM or tuning.

3.2.8: Summary of Tuning Methods

The most optimum design consists of a graded index separate confinement heterostructure - single quantum well (GRINSCH-SQW) gain region and two tuned- sampled-grating regions [24]. This approach should provide the tuning range and linewidth required to meet the 64 spot resolution required without demanding new growth, processing techniques or unduly high tuning power. If the number of resolved spots can be reduced to less than 64, a simpler two section TBF laser would meet the performance requirements with a simpler, more cost effective design.

The tuning range is an estimate of the practical maximum that might be achieved despite the fact that some higher values have indeed been reported or predicted.

3.2.9 Choice and Design of a Tunable Laser

The salient requirement of the tunable laser is to provide 64 resolvable spots. There should be 64 selectable (=tunable) discrete wavelengths sufficiently separated with respect to the linewidth of the discrete wavelengths to allow high spatial separation by a holographic diffraction grating. Similarly, the method should allow the monolithic fabrication of 32 of these lasers on a bar with each laser providing 64 spots. In addition, the need for substantial laser power output (>10 mW), low tuning power and modulation must also be considered.

A "conventional" approach using methods that did not require unusual wafer growth or processing has been chosen as the most optimum design. The tunable multisection DBR meets the requirements, but requires relatively high tuning power to achieve the necessary range. A recent report by Jayaraman, Cohen and Caldron [24] which uses a pair of tuned sampled Bragg reflecting gratings to replace the conventional tuned Bragg grating provides the required tuning range at sufficiently low tuning power to meet the program requirements. The sampled gratings give a tuning range that can be approximately 10 times larger than direct tuning of a Bragg reflector at the same tuning current or power. In addition, fabrication of the sampled grating requires only a few additional lithographic processes to be added to the fabrication of a conventional TBR laser.

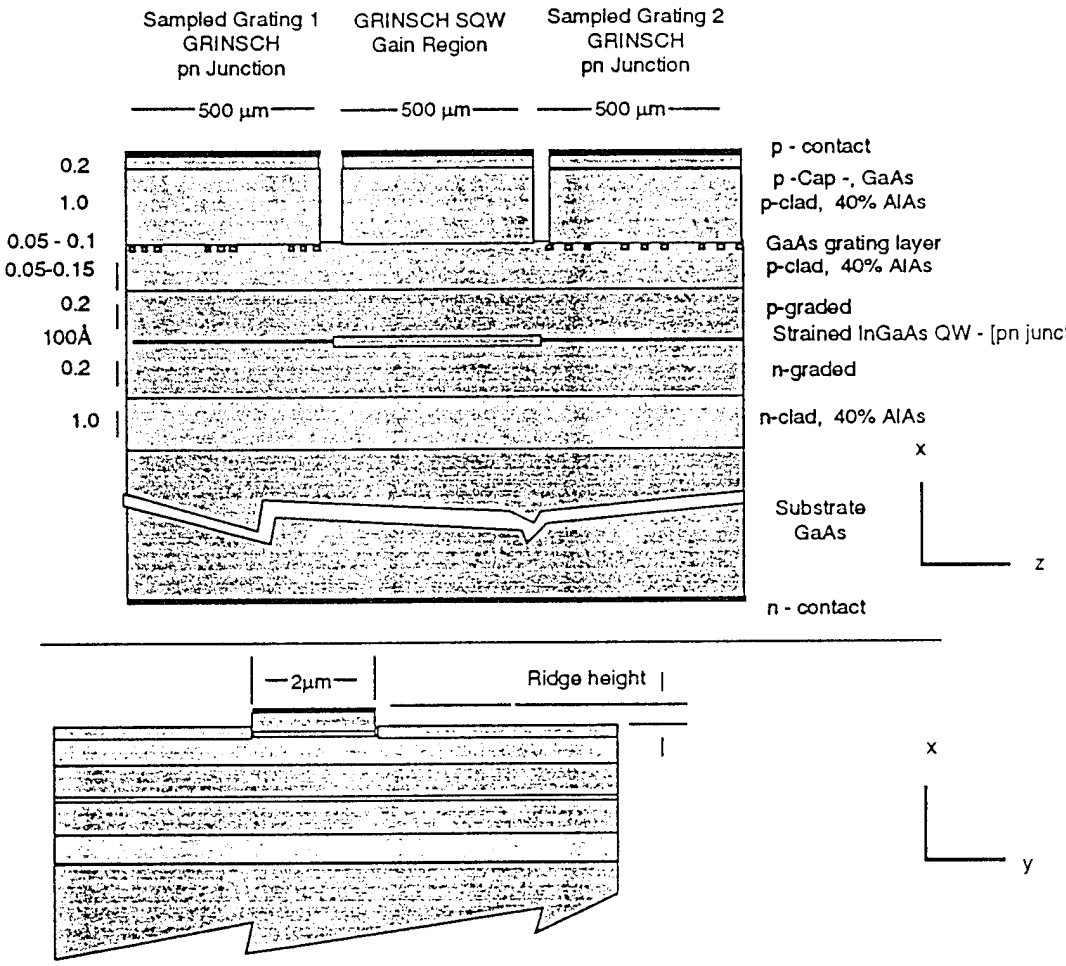

Figure 17 a) Longitudinal cross section of the proposed sampled grating structure
b) Transverse cross section of the proposed sampled grating structure

The final design is depicted in Figures 15 and 17. Figure 15a is a schematic of a sampled grating. Figure 15b is a schematic of the laser design for this program. A gain section between two tuned sampled gratings is used. Grating 1 has a sampling period L_{01}; grating 2 has a sampling period of L_{02}. The fundamental grating period Λ is chosen to reflect light at the nominal operating wavelength of the laser.

The reflectivity of the gratings as a function of wavelength is represented in Figure 15c. The reflectivity is similar in appearance to the transmission of a comb filter and consists of a series of equally spaced lines whose wavelength separation P, is a function of the sampling period. The lines are characterized by an order number, m, which we will refer to as the comb filter order. Strong reflection from both gratings is required for lasing and this occurs where an

order of grating 1 overlaps an order of grating 2. This overlap position is tuned by varying the refractive index of the gratings with injection current. The tuning will be illustrated below.

As described earlier in Equation (20), if the refractive index tuning range of one of the gratings is $\Delta n/n$, then the tuning range for this device is:

$$\frac{\Delta\lambda}{\lambda} = \frac{\Delta n}{n}\frac{P}{\Delta P}$$

As compared to a TBR with unsampled gratings, the tuning range is increased by the ratio $P/\Delta P$.

3.2.9.1 Laser Structure

As shown in Figure 17, the gain section uses a GRINSCH-SQW active region. A strained layer InGaAs quantum well operates at ≈ 950 nm. GRINSCH-SQW active structures have demonstrated gain bandwidths of 85 nm [31], which exceed the modified design specification of 64 nm. The GRINSCH-SQW has a low threshold and high efficiency with output power capabilities greater than 50 mW. Lateral confinement is proposed through a ridge guide structure. Any single-mode, index-guided structure such as a buried-ridge structure [32] or a

Table 4: Laser structure for tunable array (l ~ 0.97 μm)

Layer	Composition	Thickness
Substrate	GaAs,	~100 μm
First transition region	$Al_{0.1}Ga_{0.9}As$ to $Al_{0.6}Ga_{0.4}As$	0.1 μm
n-clad layer	$Al_{0.6}Ga_{0.4}As$	1.1 μm
First GRIN layer	$Al_{0.6}Ga_{0.4}As$ to $Al_{0.1}Ga_{0.9}As$	B (0.15 μm)
First barrier layer	GaAs	A (0.0075 μm)
Quantum well	$GaIn_{0.14}As$	C (0.01 μm)
Second barrier layer	GaAs	A (0.0075 μm)
Second GRIN layer	$Al_{0.1}Ga_{0.9}As$ to $Al_{0.4}Ga_{0.6}As$	B (0.15 μm)
First p-clad (grating spacer)	$Al_{0.4}Ga_{0.6}As$	E (0.1 μm)
First grating transition	$Al_{0.4}Ga_{0.6}As$ to $Al_{0.1}Ga_{0.9}As$	F (0.01μm)
Grating layers: [end of first growth]	**GaAs or AlGaAs (see below)**	**D (0.1 μm)**
Second etch stop transition	$Al_{0.1}Ga_{0.9}As$ to $Al_{0.4}Ga_{0.6}As$	F (0.01μm)
Second p-clad	$Al_{0.4}Ga_{0.6}As$	1.1 μm
Second transition region	$Al_{0.4}Ga_{0.6}As$ to $Al_{0.1}Ga_{0.9}As$	0.1 μm
Cap	GaAs	0.12 μm

disordered index-guide [33] could be utilized. By spacing the array elements ≈50-100 μm apart, independent addressing of each laser can be obtained without crosstalk.

The layer composition and thicknesses of the GRINSCH-SQW, specified in Table 4, are typical of wafers grown at Lincoln Laboratories and elsewhere to produce high quality lasers. The laser structure was chosen by optimizing the trade-off between having a large grating confinement factor while maintaining a reasonable quantum well confinement factor. Using computer aided design (CAD) tools, an asymmetric GRINSCH structure was chosen (typical results are shown in Figures 18, 19, 20 and 21).

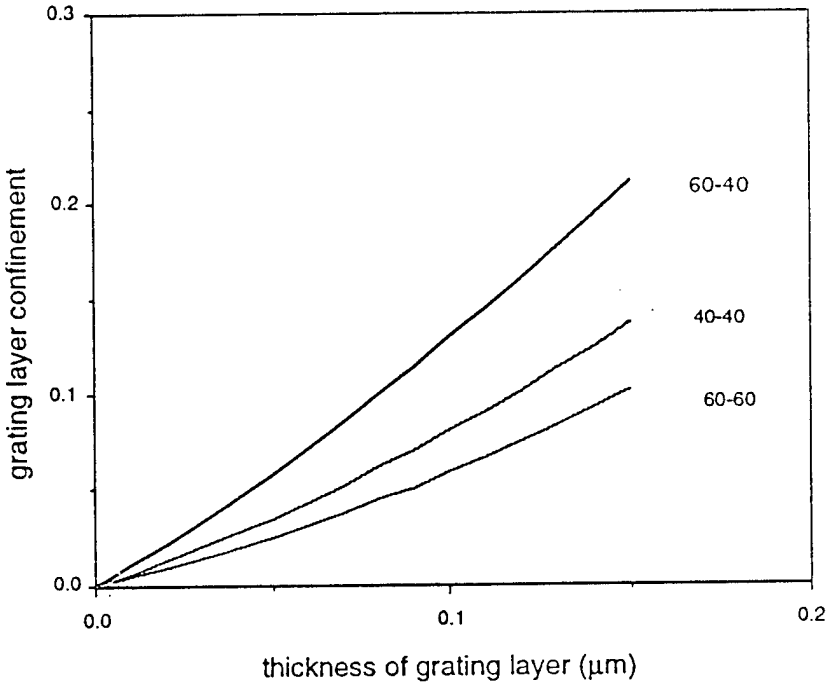

Figure 18: Grating layer confinement factor for symmetric (60-60, 40-40) and asymmetric (60-40) compositions of AlAs in the n- and p-cladding layers

Figure 18 shows the fraction of mode power (grating layer confinement factor) in the grating layer for the following n- and p- cladding regions:

60 percent and 60 percent AlAs,

40 percent and 40 percent AlAs, and

60 percent (n-cladding) and 40 percent (p-cladding) AlAs.

The grating layer confinement factor is calculated as a function of the thickness of the grating

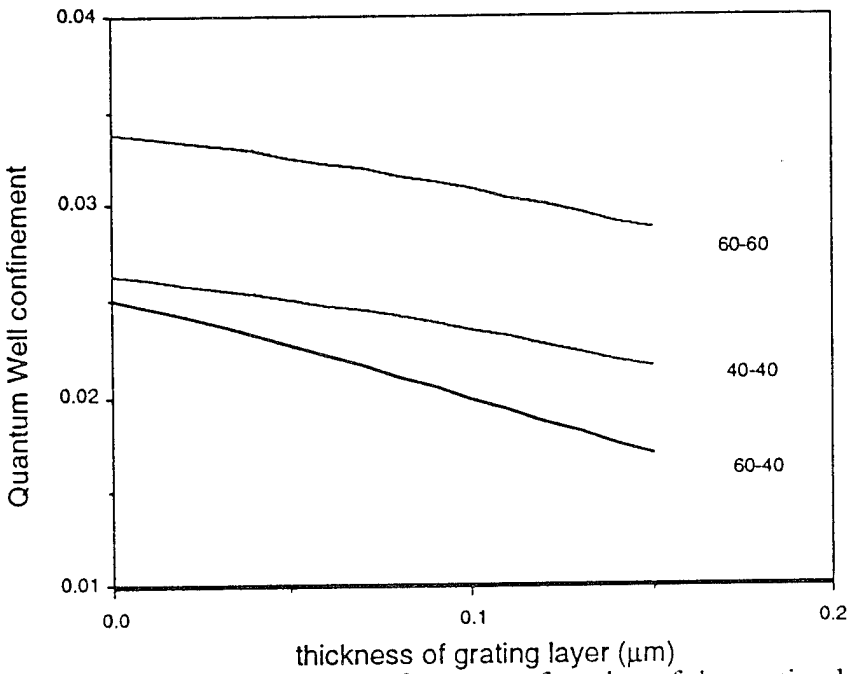

Figure 19: Quantum well confinement factor as a function of the grating layer thickness for symmetric and asymmetric cladding compositions

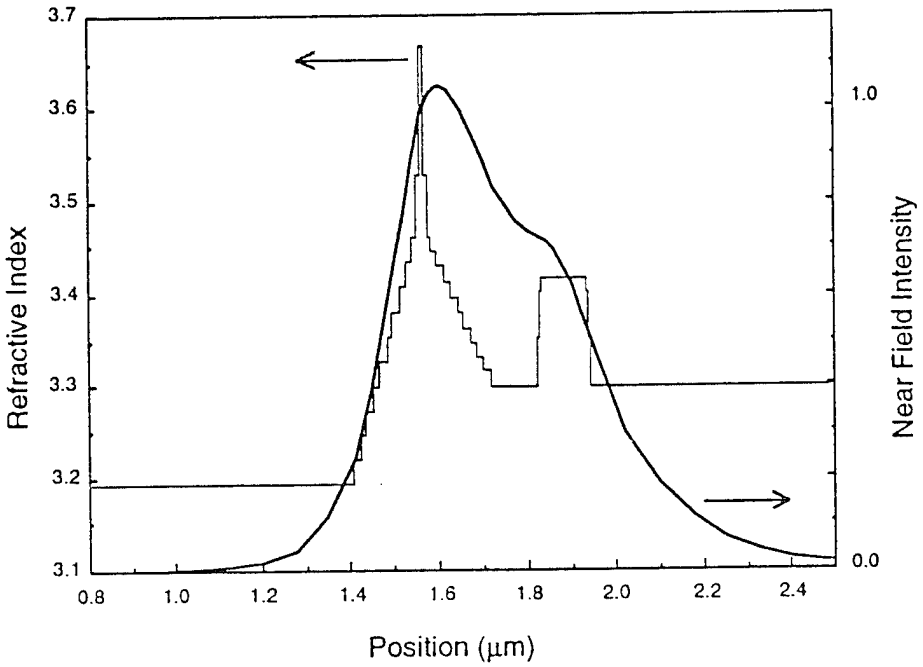

Figure 20: Index profile and near-field distribution for the layer structure for the proposed sampled-grating tunable laser

layer. The asymmetric (60-40) structure provides a larger interaction with the grating region than the symmetric (40-40 or 60-60) structures. The larger grating confinement factor is needed to obtain the grating coupling strength of ~150 cm^{-1} which is required in the sampled gratings [24]. Figure 19 shows the amount of power in the active quantum well layer for the same parameters shown in Figure 18. It also shows that a quantum well confinement factor of ~2 percent can be maintained with the asymmetric (60-40) structure with grating layers of about 0.1 μm.

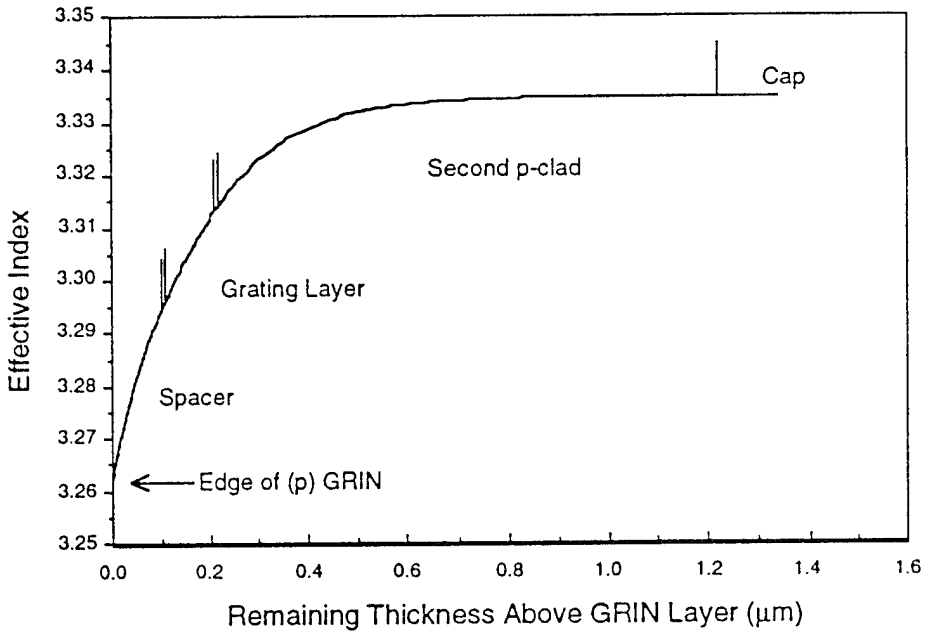

Figure 21: Effective index as a function of the remaining material above the p-graded layer for the layer structure in Table 4

The index profile of the laser structure shown in Table 4 with the near-field distribution superimposed is demonstrated in Figure 20. To obtain index guiding, the p-cap and p-clad regions are etched away to provide an index step of between 5 x 10^{-3} and 1 x 10^{-2}, which occurs when approximately 0.4 μm of material remains above the p-graded layer (Figure 21).

The GaAs p-cap and contacts layers are interrupted to define and to allow independent current injection into the two sampled grating regions. The quantum well remains in the grating regions because it will provide the current induced index changes necessary to give 64 selectable wavelengths. In the gain section, the grating layer should be removed because the losses are reduced relative to the grating sections. In addition, lower operating currents will also be realized. The GRINSCH continues throughout the device and provides the waveguide which allows almost loss-free light flow between the gain and grating regions.

The gratings are etched through a thin (<1000 Å) GaAs layer and are extended into the 40 percent AlGaAs p- clad. Generally, gratings are formed by holography to define the basic grating period Λ, and by photolithography to superpose the sampling periods L_0 and L_1. However, first order gratings with Λ=1400 Å, have been selected in the sampled grating elements to minimize losses. These gratings must be fabricated using direct-write electron beam lithography [34]. After grating formation, a 40 percent AlGaAs p- clad and GaAs regrowth is required to complete the p-cap. The p-clad thickness is a design variable which is chosen to obtain single lateral mode operation.

The ridge width design is dependent on the index step which is determined from Figure 21. The effective index of the laser mode depends on the width of the ridge. The sampled grating period Λ is determined by the lasing wavelength λ divided by the effective index n_e. Figure 22a is a plot of both the effective index and the full mode size measured to the $1/e^2$ power point against ridge width for the lowest order TE mode (labeled TE_0) with an index step of 0.01. Figure 22b shows the effective index plotted against ridge width for the lowest and first order E modes (Labeled TE_0 and TE_1 respectively). For a p-clad thickness, the ridge height was also chosen (using Figure 21) to give an effective index change of 0.01. Figures 23a and 23b are similar plots for an effective index change of 0.005. The ridge width must be ~2 μm or less for single lateral mode operation when the index change is 0.01 (Figure 22b). From Figure 23b, a ridge width of 2.5 μm can be seen to allow single lateral mode operation for an index change of 0.005. These figures again illustrate the interrelation of the design parameters.

The proposed final design is etched with a ridge of approximately 0.4 μm of material remaining outside the ridge region to give an effective index of change of 0.005 to 0.01. A ridge width of 2 μm was also chosen to ensure single spatial mode operation with a lateral mode size to $1/e^2$ of 3.3 μm. (Figure 23a). This corresponds to a mode size FWHM of approximately 2 μm.

The grating is formed in the GaAs layer which is embedded in the 40 percent AlAs material; this is regrown to a thickness of ≈ 1.0 μm to reduce the losses associated with the GaAs cap layer and contact. In this case, the ridge is formed by partially etching into the 40 percent AlAs region.

The aforementioned GRINSCH structure could be modified to produce larger carrier-induced index changes. This could be accomplished by using MQWs (3 to 5 wells) as opposed to a single quantum well. The carrier-induced index change is proportional to the number of

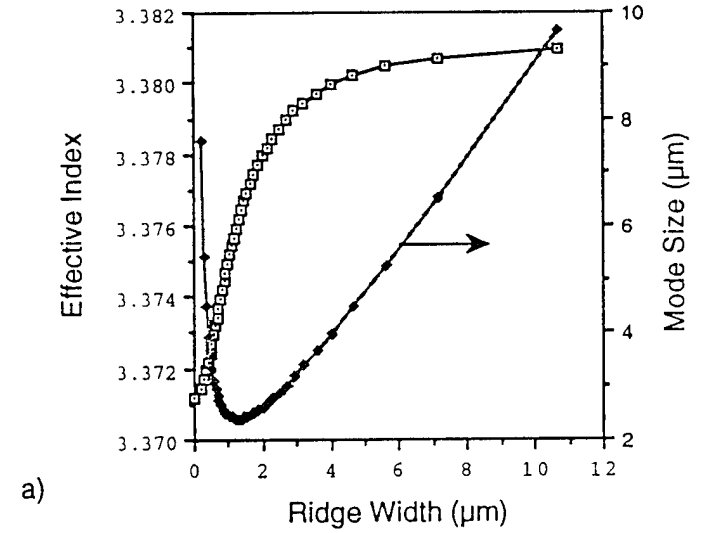

a)

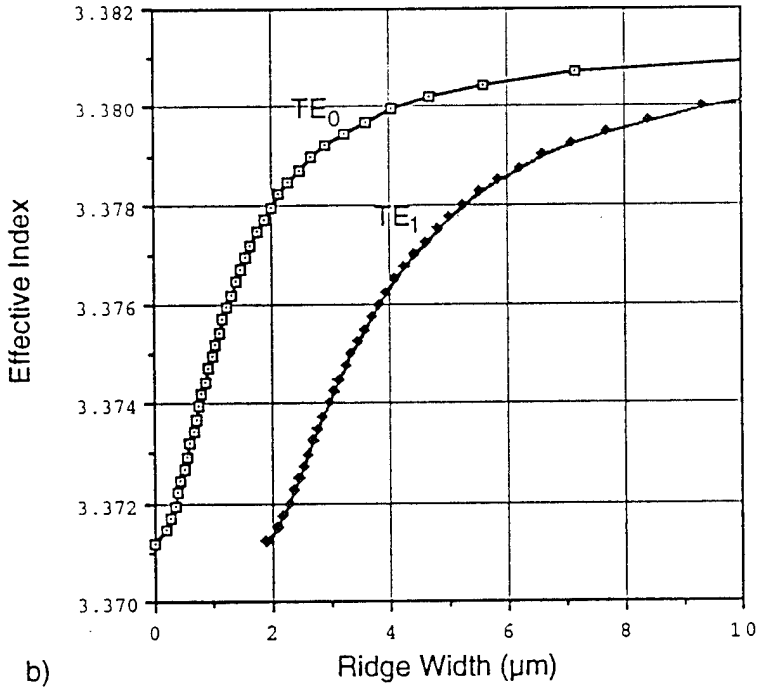

b)

Figure 22 a) Plot of both effective index and full mode size measured to the $1/e^2$ power point against ridge width for the lowest order E mode (labeled TE_0)
b) Effective index plotted against ridge width for the lowest and first order E modes (labeled TE_0 and TE_1 respectively) for an effective index change of 0.01

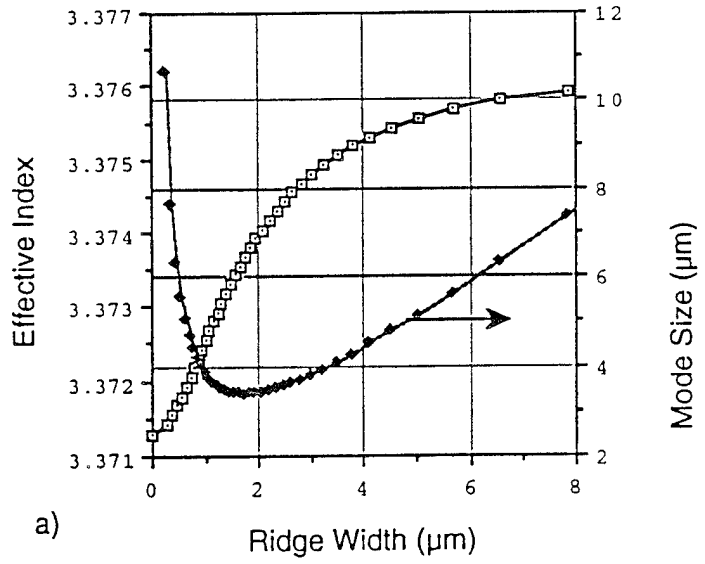

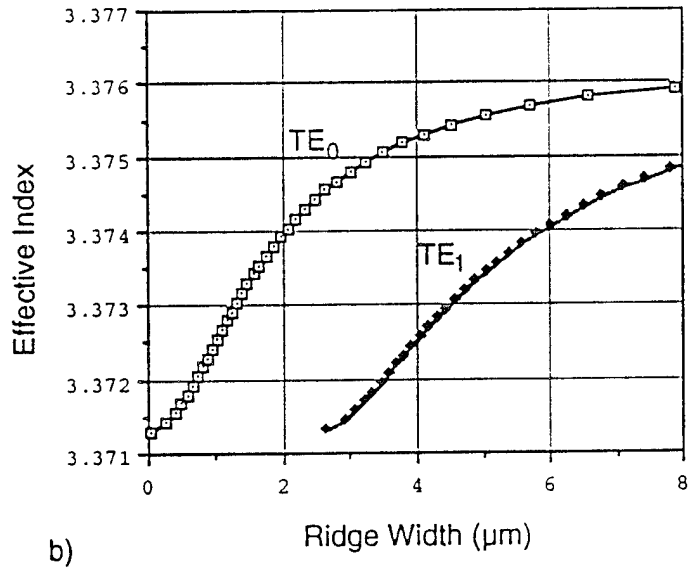

Figure 23 a) Plot of both effective index and full mode size measured to the $1/e^2$ power point against ridge width for the lowest order E mode (labeled TE_0)
b) Effective index plotted against ridge width for the lowest and first order E modes (labeled TE_0 and TE_1 respectively) for an effective index change of 0.005

quantum wells. This should be an advantage in wavelength-tunable laser designs where it is desirable to obtain a maximum wavelength shift with a minimal current change. Three quantum well active layer InGaAs/GaAs lasers have exhibited thresholds of less than 10 mA [31], which is comparable to the best SQW-GRINSCH lasers. It is possible that such low thresholds could be obtained with as many as 5 wells, but this needs to be experimentally verified. In adding more wells, it will be necessary to reduce the thickness of the GRINSCH layers to maintain the proper grating confinement. This is a minor structural change that would be made once the exact structure of the multi-quantum well layer had been determined.

3.2.9.2 Sampled Gratings—Dimensions and Mode Spacing

On the basis of the results obtained from Jayaraman, Cohen and Coldren [24], 500-μm-long sampled gratings were initially chosen with sampling periods L_{01} and L_{02} of 40 and 45 μm, respectively. The length, L_1, is a parameter that is significant in the control of the sharpness of the comb filter reflection lines (Jayaraman et al. used 5 μm). The wavelength values of the lines of the two gratings is given by:

$$\lambda_1 = 2(n_e + \delta n_1)\Lambda\left(1+\frac{m_1\Lambda}{L_{01}}\right) \quad (21)$$

$$\lambda_2 = 2(n_e + \delta n_2)\Lambda\left(1+\frac{m_2\Lambda}{L_{02}}\right) \quad (22)$$

$$m_1, m_2 = 0,1,2,,3\text{------}$$

where m_1 and m_2 are the "comb filter" orders, and δn_1 and δn_2 are the pumped change in refractive index of the two gratings. Some values of δn_1, δn_2 and the resulting overlap wavelengths $\lambda_1 = \lambda_2$ (= overlap λ) for $m_1 = -1$, $m_2 = 0$ and for $m_1 = 0$ and $m_2 = 1$ are listed in Table 5 to illustrate the tuning capabilities of this approach.

Similar calculations for other orders show increased tuning with smaller refractive index changes for switching between high "comb filter" orders. For example, $m_1 = 1$, $m_2 = 2$, $\delta n_1 = 0.002$, $\delta n_2 = 0.01$, $\lambda = 9611$Å; for $m_1 = 2$, $m_1 = -1$, $\delta n_1 = 0.008$ $dn_2 = 0.005$, $\lambda = 9500$ Å for a total range of 111 Å. This tuning range, which requires a total variance in n of less than .01, is adequate to resolve 128 spots at the equivalent fp mode spacing of $\Delta\lambda = 0.844$ (calculated from Equation 2b) which requires 108 Å. A total variance in n {Max (dn_1:dn_2) at λ_{max} - Max (δn_1:δn_2) at λ_{min}} of less than 0.01 can be used. Under optimal conditions such variations have

been observed with currents less than 100 mA. From Jayaraman et al's work [24], 293 Å of tuning is observed with a maximum current range of 86 mA.

Table 5: Example of sampled grating tuning where: λ_0=9550 Å, n_e = 3.6, Λ = 1,326 Å (1st order Bragg Reflector), L_{01} = 40 μm, L_{02} = 45 μm

"Comb filter" order m_1=0, m_2=1			"Comb filter" order m_1=-1, m_2=0		
dn_1	dn_2	Overlap l(Å)	dn_1	dn_2	Overlap l(Å)
δn_1	δn_2	9551.5	δn_1	δn_2	9496.9
-0.005	0.0055	9564.8	-0.012	0	9518.2
-0.004	0.0065	9567.5	-0.005	0.007	9536.7
-0.003	0.0075	9570.2	-0.004	0.008	9539.4
-0.002	0.0085	9572.8	-0.003	0.009	9542.0
-0.001	0.0095	9575.5	-0.002	0.010	9544.7
0	0.0105	9578.1	-0.001	0.011	9547.3
0.001	0.0115	9579.5	0	0.012	9550.0
0.002	0.0125	9583.5	0.001	0.013	9552.7
0.003	0.0135	9586.1	0.002	0.014	9555.3
0.004	0.0145	9588.8	0.003	0.015	9558.0
0.005	0.0155	9590.1	0.0009	0.020	9573.9
0.009	0.0200	9602.1			

Section 4.0: Chromatic Dispersion Analysis

At the outset of the program, it became readily clear that the planar wave guide approach or any thin film approach (T < 20 μm) would not be desirable except in a limited class of applications. This limited class includes high speed scanning (<1ns/pixel) and low density read only memory access (~4-16k bit). For high density memory systems, efficient selectivity is required. The film loses diffraction efficiency as the memory density is increased. The original PROMAC concept used the tunable laser to illuminate a planar waveguide grating which subsequently illuminated some form of optical memory. The planar waveguide grating dispersed the incident radiation at an angle proportional to the wavelength by which it was illuminated. By

changing the wavelength, angular scanning may be accomplished as demonstrated in the laboratory proof-of-principle which was fabricated and documented in Section 3 of this report.

Originally, it was felt that angular scanning would be used to address various spatial locations on a plate or disk. Therefore, the number of storage bits would be limited to the number of resolvable spots or angles, times the number of bits illuminated in each location of the plate or disk. This method is detection limited because the number of bits illuminated in each location of the plate or disk is limited to several hundred to a thousand (bits) at speeds between 1 to 10 ns. The tunable lasers are limited to a few hundred hops under the most optimistic arrangement. It is conceivable that an array of lasers could be configured to illuminate a 2D array of 1000 point images. The maximum practical memory size for such a system would approach approximately 10E8. For many applications, this may be sufficient. Note that a 2D array of lasers does not lend itself to practical implementation.

It may be prudent at this time to reconsider an old concept, which at the time of its invention lacked an appropriate read mechanism, namely volume holographic storage. If properly implemented, 2 to 3 orders of magnitude in storage capacity may be achieved with read speeds on the order of nanoseconds with DBR tunable lasers. If a volume crystal has a thickness T and a reference beam angle (in air) of 60 degrees (θ), then the diffraction efficiency equation of a thick volume material is given by the following equation:

$$\eta = \frac{\mathrm{Sin}^2(\xi^2 + \nu^2)^{1/2}}{(1 + \xi^2/\nu^2)} \qquad (23)$$

This equation originally was developed for thick materials by H. Kogelnik, "Coupled Wave Theory for Thick Hologram Gratings," Bell. Syst. Tech. J. 48, 2909, (1969). The two diffraction parameters ξ and ν are described by the following two Kogelnik equations:

$$\xi = -\frac{\Delta\lambda}{\lambda_a} \mathrm{Tan}\,\theta_0 \left(\frac{2\pi n_0}{\lambda_a}\right) T \,\mathrm{Sin}\,\theta_0 \qquad (24)$$

where: $\nu = \frac{\pi}{2}$ (25)

The first variable ξ, is described as the thickness T, reference beam angle θ, and center frequency or color, λ. The variable plotted in Figure 24 is diffraction efficiency η as a function of $\Delta\lambda$ where the parameter ν has been artificially frozen at $\pi/2$ which is the condition of 100% modulation. It is referred to as the modulation parameter.

In Figure 24, the following assumptions are made:

T =3.4 mm (a reasonable thickness for the material)

λ = 1 μm, and

n_o (index of refraction) = 1.52.

The index of the material is important because θ must be compensated within the crystal. Under these conditions, the first null of the diffraction efficiency occurs at 7 Å away from the center frequency of the laser.

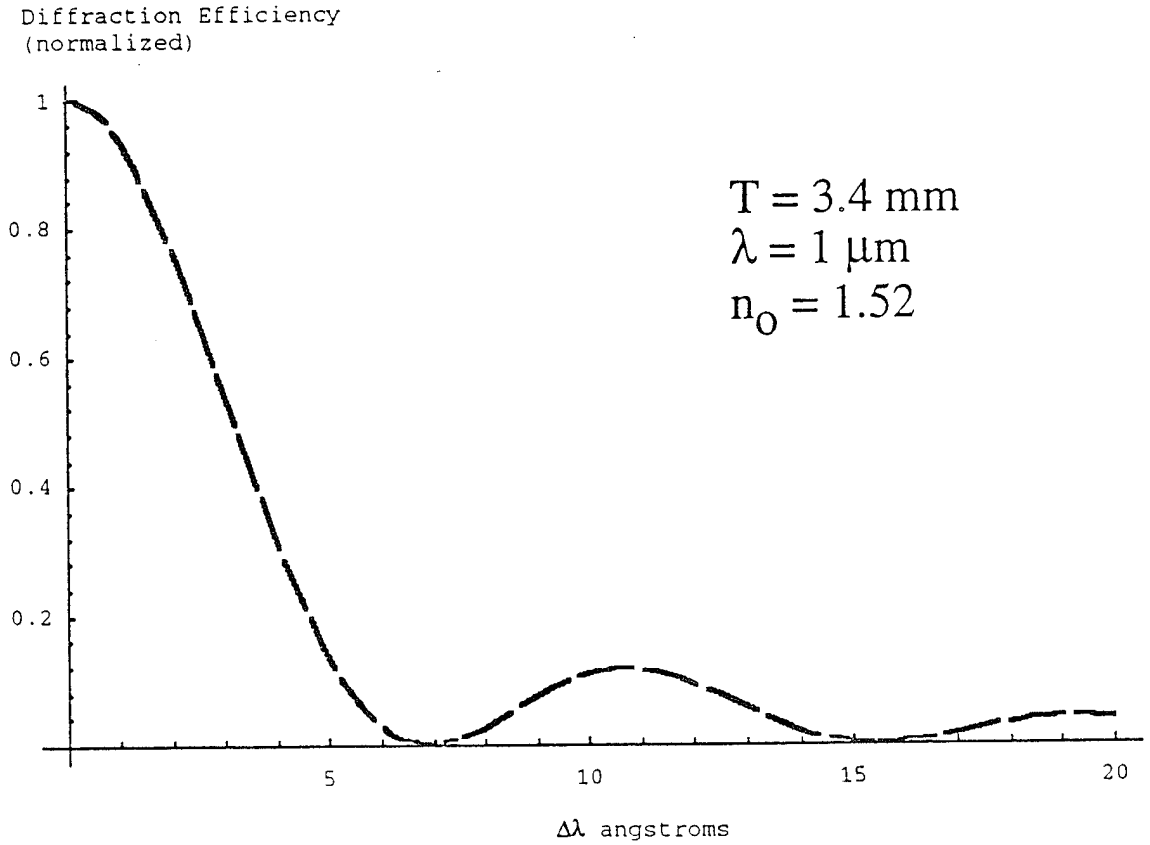

Figure 24: Normalized diffraction efficiency of a thick material at 1 μm wavelength and a thickness of 3.4 mm. The first null is located at 7 Å from the center frequency of the laser.

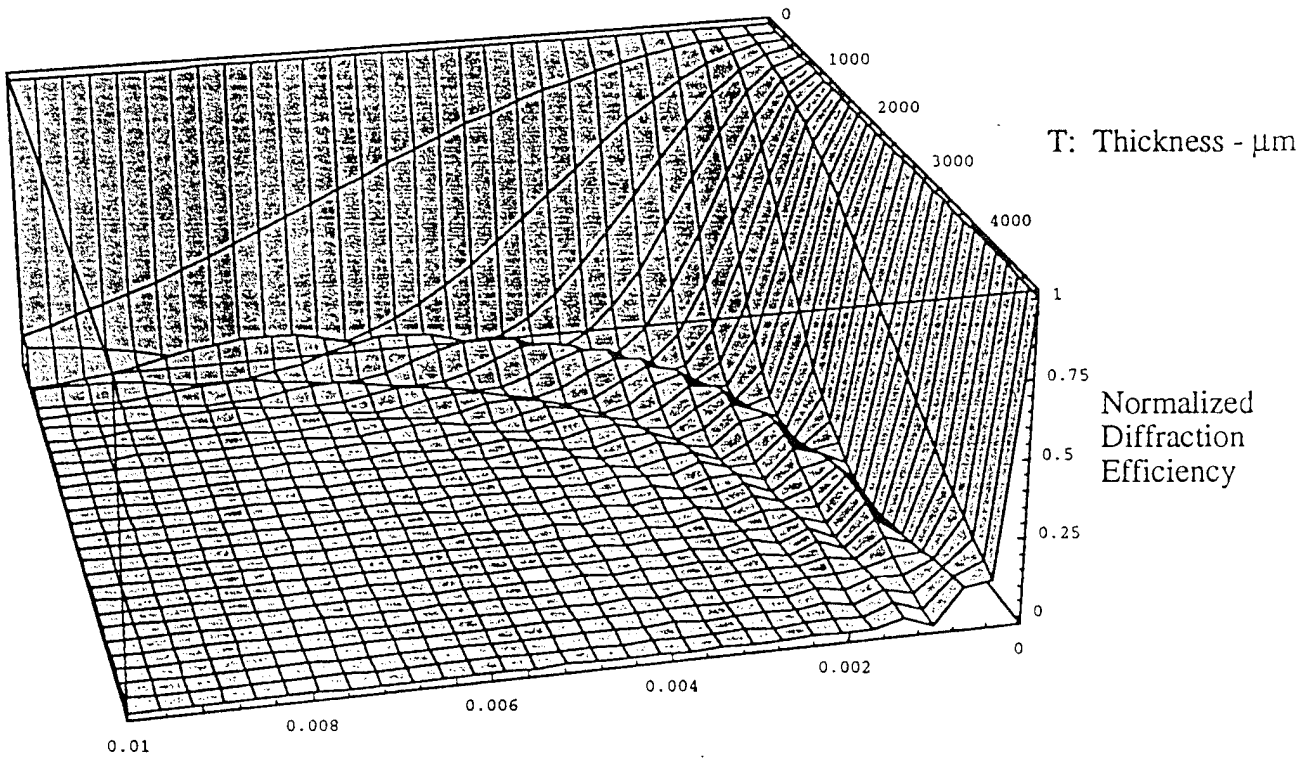

Figure 25: 3 dimensional plot of volume interconnect diffraction efficiency, spectral resolution and thickness

The same equation is plotted in multi dimensions as shown in Figure 25. The first null in the figure defines the spectral resolution requirement to isolate with sufficient crosstalk minimization adjacent holograms in a thick material. This is extremely important because all of the energy from the laser will couple into the appropriate data pattern stored. In a thin material, the motion is continuous and therefore, extremely lossy. The energy can be directed into a given memory plane or location volume. Note that at 1 μm, the thickness is substantial for small $\Delta\lambda$s.

The first null by itself may be plotted by setting the diffraction efficiency equal to zero and solving for $\Delta\lambda$ where the following equation is obtained:

$$\Delta\lambda = \frac{2}{\sqrt{3}} \lambda^2 \{\text{Tan}\,\theta_0\,(2n_0)\,T\,\text{Sin}\,\theta_0\}^{-1} \qquad (26)$$

Reasonable tunable laser designs are in the 1 μm region. The plot of the first null of the diffraction efficiency as a function of $\Delta\lambda$ and the thickness of the crystal is shown in Figure 26. In all cases, the reference beam angle in air has been assumed to be 60 degrees. The material has to be substantially thick (8 - 15 mm) to obtain null rejection of adjacent modes in the 2 - 5 Å regime.

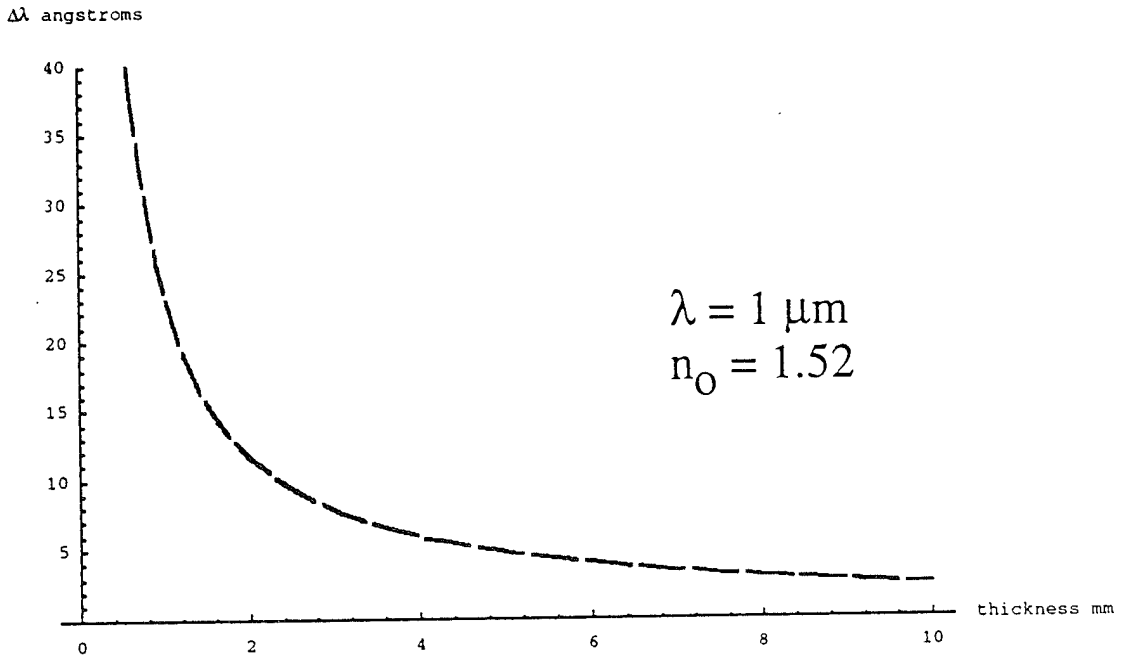

Figure 26: Volume interconnect -- spectral resolution vs. crystal thickness at $\lambda = 1\ \mu m$

However, if a laser can be designed with $\Delta\lambda$ on the order of 10 Å or greater, then the thickness requirement on the crystal becomes reasonable, in the 1 to 3 mm range.

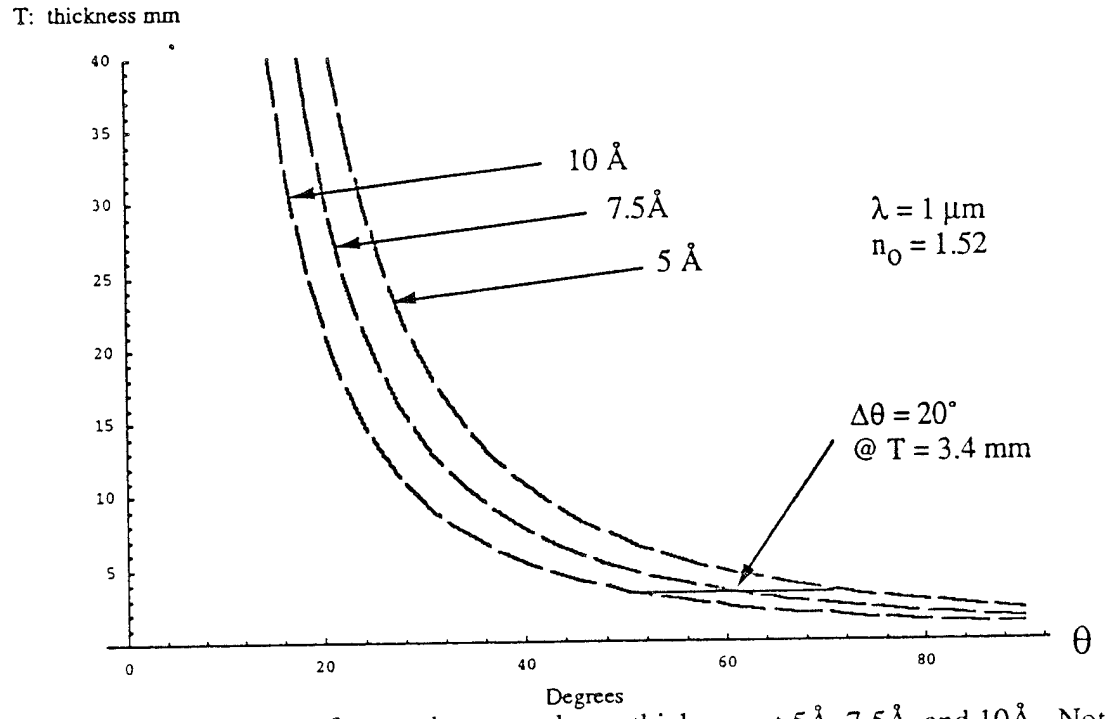

Figure 27: Free space reference beam angle vs. thickness at 5Å, 7.5Å, and 10Å. Notice the variance between 5Å and 10Å grows to 20 degrees at T = 3.4 mm.

The thickness of the crystal is not only a function of the spectral mode separation but also the reference beam angle as described in Figure 27. The figure is plotted by solving the diffraction efficiency equation (27) for thickness where the following expression is obtained:

$$T = \frac{2}{\sqrt{3}} \lambda^2 \{ \text{Tan}\, \theta_0 \, (2n_0) \Delta\lambda \, \text{Sin}\, \theta_0 \}^{-1} \qquad (27)$$

A primary objective is to minimize the thickness of the crystal and the reference beam angle. Consequently, the larger the mode separation on the tunable laser, the better the performance. We have chosen 10Å mode hops over a 64 nm range centered at 950 nm. The design of this laser represents a significant utilization of the most advanced DBR laser technology. To date, a 24 nm bandwidth has been demonstrated. It is apparent that for the proposed application (as in most), ~10% fractional bandwidth is required (which is actually only 6.4%). The state of the art has achieved 2.5%. The gain curve of a typical laser diode will support 10% fractional bandwidth. Although tuning ratio requirements are severe, it is felt that they are achievable.

5.0 Design for a 10 Å, 64 Hop Wavelength Tunable Laser

The specifications for the wavelength tunable laser were modified to 64 selectable wavelengths with a wavelength separation of 7 to 10 Å between adjacent wavelengths. A nominal operating wavelength of about 9500 Å is desired. Therefore, the tunable laser must operate over a wavelength range from about 9180 Å to 9820 Å. Another goal is to only use two current controls to select the wavelengths. A design in the InGaAs/GaAs materials system has been developed that will provide ≥ 64 selectable wavelengths, separated by ~ 10 Å. Furthermore, only two current controls are needed to select any wavelength.

5.1 Integration of Sample Gratings

The favored design approach is to use electronically tunable sampled gratings as the end reflectors for the semiconductor laser element. This new approach was first demonstrated by Jayaraman et al. [24] in May, 1992. By using sampled-gratings (with slightly differing sampling periods), wavelength tuning ranges as high as 63 nm have been obtained in InGaAsP /InGaAs @ 1.55 μm. To arrive at a design for a wavelength-tunable sampled-grating laser in the InGaAs/GaAs at 0.95 μm with 64 selectable wavelengths, Jayaraman et al.'s [24] approach has been improved by including the effects of the current-induced changes in the refractive index. The amplitude reflectivity for a sampled grating is:

$$r(\lambda) = \sum_{n=-\infty}^{\infty} \frac{i\kappa^*(n) \sin[q(n)L]}{q(n)\cos[q(n)L] - i\Delta\beta \sin[q(n)L]} \qquad (28)$$

where the de-tuning, $\Delta\beta$, is:

$$\Delta\beta = \frac{2\pi\mu(I,\lambda)}{\lambda} - \frac{\pi}{\Lambda} - \frac{\pi n}{Z_0} + \frac{i\alpha}{2} \tag{29}$$

and α is the power loss coefficient, n is the diffraction order, Λ is the grating period, Z_0 is the sampling period length, and L is the total length of the sampled grating. The effective index $\mu(I,\lambda)$, which is dependent both on current, I, and operating wavelength, λ, is :

$$\mu(I,\lambda) = \mu(I_0,\lambda_0) + \frac{\partial\mu}{\partial I}(I - I_0) + \frac{\partial\mu}{\partial\lambda}(\lambda_0 - \lambda) \tag{30}$$

where I_0 and λ_0 are arbitrary current and wavelength references. The functions $\kappa(n)$ and $q(n)$ are:

$$\kappa(n) = \frac{\kappa_0 Z_g}{Z_0} \frac{\sin(\pi n Z_g/Z_0)}{n Z_g/Z_0} \exp(i\, n Z_g/Z_0) \tag{31}$$

and

$$[q(n)]^2 = [\Delta\beta(n)]^2 - |\kappa(n)|^2 \tag{32}$$

where κ_0 is the coupling coefficient of the unsampled grating.

Using Equations (28) - (32), the following set of parameters for the sampled gratings are: $\Lambda = 0.144$ μm, $Z_{01} = 16.5$ μm, $Z_{02} = 18.5$ μm, $Z_g = 1.5$ μm, $L_1 = 1000$ μm , $L_2 = 500$ μm, $\alpha = 10$ cm^{-1}, $\lambda_0 = 0.95$ μm, and $\kappa_0 = 150$ cm^{-1}. The power reflectivity bandwidth spans the desired ~ 60 nm tuning range. This is illustrated in Figure 28, where the peak-power reflectivity (at the Bragg wavelengths) is plotted as a function of the Bragg wavelength corresponding to the grating orders m = ±5, ±4, ±3, ±2, ±1, 0. Note that only the peak reflectivity is shown. There are side lobes in the power reflectivity. For grating order, the first side lobes are spaced roughly at ±1000 Å with a peak reflectivity of less than 0.03. Because the gain bandwidth of the semiconductor medium is less than 1000 Å, these low reflectivity side lobes should have a negligible effect on device performance. From Equation (28), the FWHM reflectivity bandwidth of each order is calculated to be less than 2 Å. Sampled grating 1 ($Z_{01} = 16.5$ μm) acts as a high reflector (relatively speaking) and has a length of 1000 μm. Sampled grating 2 ($Z_{02} = 18.5$ μm) at the output end has a length of 500 μm. For this example, $\mu(I,\lambda) = \mu(I_0,\lambda_0) = 3.3$ was selected

because this is consistent with the InGaAsP/GaAs material system. At this operating point, the reflectivity curves in Figure 28 overlap only at the m = 0 order, which corresponds to a wavelength of 9503 Å. None of the other orders overlap.

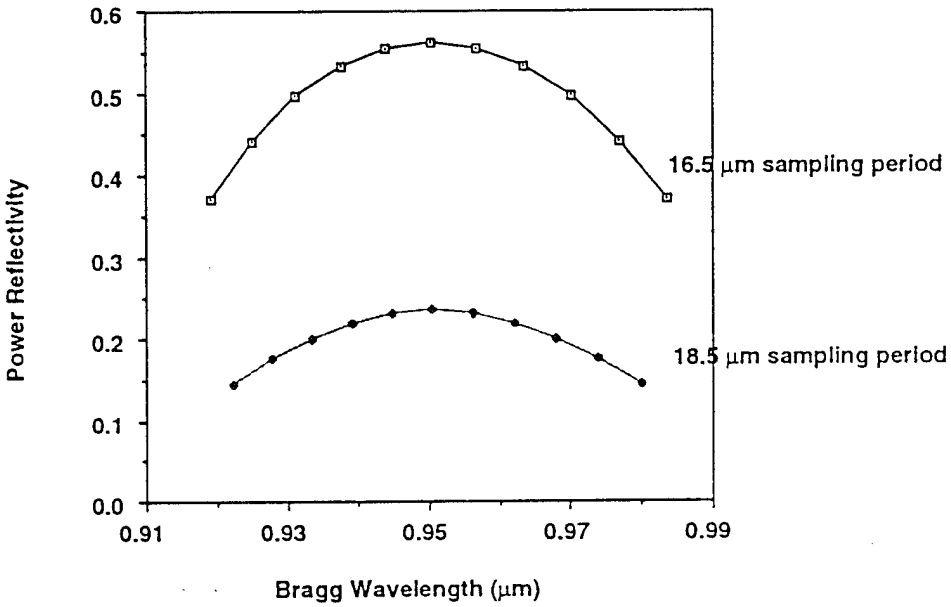

Figure 28: The peak power reflectivity vs Bragg wavelength is plotted for the proposed sampled gratings.

5.2 Operating Wavelength

The wavelength-tunable laser comprises the aforementioned sample gratings integrated onto the ends of a gain section (without grating) with any of the transverse and lateral structures that are described in Section 3.2.9.1. The gain section length is selected to be 300 μm. This gives a longitudinal mode separation of 3.6 Å, which ensures single-mode operation within the reflection bandwidth of each order of the sampled gratings. The sampled gratings themselves are active devices. By varying the current to each electrode, the comb of reflection peaks (Figure 28) are scanned relative to each other so that a different set of orders overlap. Hence, laser operation occurs at the new wavelength. The wavelengths at the peak reflectivities of a sampled grating are:

$$\lambda (I_j, m_j) = \mu\left(I_j, \lambda (I_j, m_j)\right) \left(\frac{\Lambda Z_{0j}}{Z_{0j} + m \Lambda}\right) \tag{33}$$

where j = 1,2 corresponds to the sampled gratings at the ends of the laser. Laser operation occurs only at those current values and grating orders where:

$$\lambda (I, m_1) = \lambda (I + \delta I, m_2) \tag{34}$$

In this equation $I = I_1$ and $\delta I = I_2 - I_1$.

From Equations (30), (33), and (34), the allowed operating wavelengths are determined not only by the current difference δI, but also by the magnitude of the current to each sampled grating. For example, with a fixed I, there is a discrete set of values of δI, that will give overlap of the Bragg orders. The current-induced index change required to switch laser operation between adjacent grating orders when $m_1 = m_2$ is approximately 0.003, which corresponds to $\delta I \sim$ 30 mA for a SQW structure and $\delta I \leq 10$ mA for a MQW structure. The condition that $m_1 = m_2$ gives the largest tuning range and smallest current-induced index change. As shown in Figure 28, this will provide 11 independent wavelengths (corresponding to $m_1 = m_2 = \pm 5, \pm 4, \pm 3, \pm 2, \pm 1, 0$) which are separated by about 60 Å, and will be referred to as the coarse wavelength selection. To obtain the higher degree of selectivity necessary for 64 independent wavelengths, it will be necessary to vary I so that the absolute position of the overlap is also varied. The analysis shows that a 0.004 change in the index, μ, is required to give ~10 Å absolute shift in the grating-order overlap wavelength. To obtain the required 64 selectable wavelengths, 6 different values of I are needed.

In Figure 29, the operating wavelength versus overlapped grating order number is plotted. There are 66 points corresponding to the selectable operating wavelengths. Coarse wavelength selection between grating orders (horizontal axis in Figure 29) is provided by tuning δI, and fine wavelength selection (vertical axis) is provided by tuning I. Figure 30 shows an enlarged view of the long-wavelength end of the scan to illustrate that the fine wavelength intervals correspond to about 10 Å. In the 500-μm sampled grating, it is estimated that each 10 Å wavelength change will require about 30 mA current change for a SQW structure and ≤10 mA current change for a MQW structure. For the 1000 μm sampled grating section, these values for the current change would be doubled.

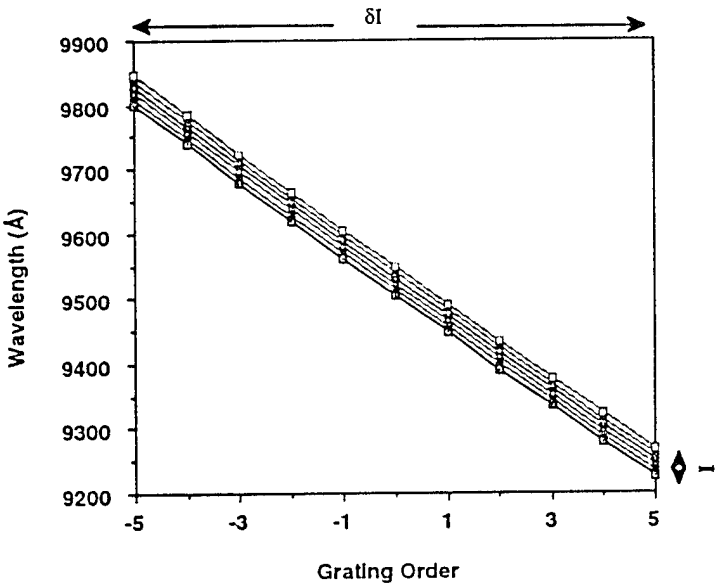

Figure 29: The operating wavelength versus order number are plotted on a coarse wavelength scale. Each operating wavelength is represented by a point; because of the coarse resolution of the vertical axis, it is difficult to resolve fine tuned wavelengths.

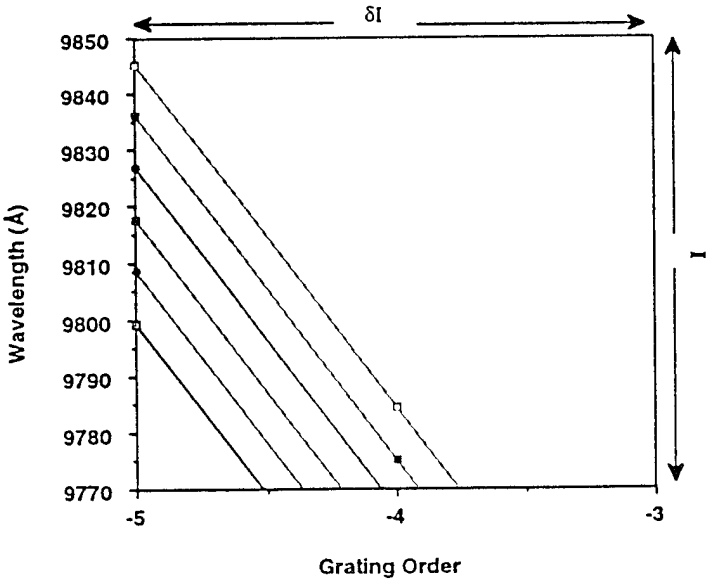

Figure 30: A portion of the operating wavelength versus order number are plotted on a fine wavelength scale. Each point corresponds to an operating wavelength. Adjacent points are separated by ~ 10 Å.

5.3 DBR Laser Design Summary

The requirement for 64 selectable wavelengths may lead to maximum operating currents of several hundred mA. The refractive index change with temperature in semiconductor lasers is $\delta\mu/\delta T \approx 4 \times 10^{-4}\ ^{\circ}C^{-1}$ where $\delta\mu/\delta T$ is positive and $\partial m/\partial I$ is negative, so that with increasing current, the temperature-induced index change will partially compensate the current-induced index change. The proposed design is based upon current-induced index changes of 0.004, which would be canceled out by only a 10 °C rise in temperature.

A thermally optimized structure, as well as a packaging architecture and thermal management system that provides maximum heat removal, is required [35-37]. Even using the most aggressive thermal packaging, it is likely that the active layer could experience a ~25°C change in temperature over the range of anticipated operating currents. This would correspond to a temperature-induced index change of 0.01. Obviously, this index change would have a significant effect on the wavelength tuning characteristics, reducing the wavelength scanning range below the desired 64 nm. Although, MQWs have larger current-induced index changes than SQW lasers, they also have higher threshold currents. An experimental study of current-induced index changes, wavelength tunability, and heat dissipation versus number of QWs in InGaAs/GaAs lasers should be performed to verify a thermally-optimized design. The current-tuning algorithm would have to be modified to account for thermal effects. As the thermal effects are primarily controlled by the heat sinking, thermal management and packaging is a critical design issue. The thermal packaging that is likely to be needed has been developed and is available from both Lawrence Livermore Labs as well as MIT Lincoln Labs.

The level of heat dissipation can limit the wavelength tuning range. The thermal tuning effects could be compensated somewhat by modifying the periods of the sampling grating. However, the thermal properties of the laser and associated packaging must be completely characterized before this can be considered.

The choice of the lateral structure also impacts heat removal. Both the buried-ridge guide[33] and the disordered index guide [34] have superior thermal characteristics to the proposed ridge guide, but both are considerably more difficult and more costly to fabricate than the ridge guide. However, if the thermally optimized transverse epilayer structure of the laser did not provide sufficient wavelength tuning range, then it would be necessary to use either the buried-ridge guide or the disordered index guide.

When fabricating an individually-addressable, monolithic 32 element array of wavelength selectable lasers, the material and process should be sufficient to give a high yield of devices that operate within the specified wavelength range. Generally, a10 Å variation occurs over a 1 cm length in DBR lasers. At 10 Å, the proposed design will provide approximately 66 spots. The extent of the 32 element array should be less than 1 cm. However, if the current levels can be kept low enough, a 10 Å spread should be controllable by appropriately adjusting the currents to each device.

Non-uniformities in the sampled grating will be manifested as reductions in the peak reflectivities and as the appearance of spurious side bands in the power reflectivity. To address this issue, a detailed experimental study of sampled grating reflectors (fabricated by direct write e-beam) should be performed to determine if suitable power reflectivity characteristics can be obtained. Once a thermally-optimized laser structure has been determined (for both transverse and lateral structures), and the power reflectivity characteristics of the sampled grating have been verified, then it would be possible to fabricate a single array element.

6.0 Volume Holographic Optical Interconnect Element (V-HOIE)

A major objective in developing an efficient architecture is the design of the photorefractive volume holographic optical element. In order to realize an optimal wavelength selective interconnect pattern, 64 volume holograms addressing 64K points (1000 points per hologram) in a 300 μm x 300 μm x 2-3 mm volume need to be superimposed and arranged in a regular array. Patterns will be selected by wavelength tuning of the infrared signal beam at intervals of 10 angstroms. The interconnect elements are 300x300 micron in lateral dimension and 2-3 mm thick. Consequently, the recording medium should allow:

- Readout in the near infrared wavelength range
- Fixing of interconnect patterns
- Near diffraction limited performance, with an impulse response of 32x32 microns.
- Low noise and crosstalk between interconnect patterns

Mathematically, the superposition of multiple interconnect patterns is described using the Born approximation:

$$\tilde{S}_c(k_x, k_y) = i \frac{n_1}{I_0} \frac{\pi}{\lambda} L \int dk_z \exp[-i\,\Omega(\mathbf{k})\frac{L}{2}]\,\mathrm{sinc}[\Omega(\mathbf{k})\frac{L}{2}] \times [\hat{S}_w * (\hat{R}_w \star \hat{R}_c)](\mathbf{k}) \quad (35)$$

$$[\hat{S}_w * (\hat{R}_w * \hat{R}_c)](\mathbf{k}) = \int d^3\mathbf{k}' \int d^3\mathbf{k}'' \, \hat{S}_w(\mathbf{k} - \mathbf{k}') \, \hat{R}^*_w(\mathbf{k}'' - \mathbf{k}') \, \hat{R}_c(\mathbf{k}'') \tag{36}$$

$$\Omega(\mathbf{k}) = \frac{k^2 - \beta^2}{2k_z} \tag{37}$$

where $\tilde{S}_c(k_x, k_y)$ denotes the reconstructed wave field, n_1 is the index perturbation, I_0 a proportionality constant, λ the wavelength, L the interaction length, k_z the k-vector component in the z- direction, Ω the dephasing factor, $\hat{S}_w$ the signal wave during recording, and $\hat{R}_w$ and $\hat{R}_c$ the reference wave during recording and readout, respectively, and k and β are wave vectors.

The equation states that the diffracted beam efficiency depends on the index modulation, which is related to the electro-optic properties of the medium, the interaction length L, and the integral involving the cross correlation between the recording and readout reference beam convolved with the signal beam. This is multiplied by a phase factor dependent on the interaction length. A sinc function that depends on the dephasing factor and the interaction length of the medium modulates the result. Crosstalk results from Bragg degeneracy and mismatch between spatial frequency components as expressed by the convolution and cross correlation terms in the integral. The Bragg selectivity is expressed by the sinc term, which allows multiplexing of holograms. Using this model, we can compute crosstalk and signal-to-noise ratios for a particular recording geometry and materials response. It is recommended that this approach, which was recently described by Bradshaw et al, in 1993, will be used as a framework for designing the interconnect array.

There are several critical issues to be investigated to optimize the superposition of multiple interconnect patterns. The following summary briefly describes the most important parameters.

6.1 Materials Issues

The first area of concern is the wavelength sensitivity range of suitable photorefractive crystals. Volume Bragg holograms have strong wavelength and angular selectivity allowing multiple holograms to be superimposed without much crosstalk. However, this also requires that

either the interconnect patterns are recorded with the same wavelength as used during readout, or by predistorting the patterns to account for the wavelength change between recording and readout. The first approach is preferred, but this requires that the recording medium must be sensitive in the near infrared region (IR) of the spectrum. Most photorefractives of interest such as LiNbO3 and SBN are not sensitive in the IR, although a recent report indicates that perhaps suitable dopants may be added to LiNbO3 to extend the sensitivity range to 0.8-1 micron regime. Unfortunately, this work was carried out in China; and, to date, no details are available. Heavily Ce doped SBN may also be an appropriate choice, but little experimental evidence for operation in that wavelength range is known.

Alternatively, the interconnect patterns may be predistorted during the recording process allowing recording at visible wavelength and readout in the near IR. To achieve good spatial resolution the distortions introduced by the wavelength shift between recording and readout are compensated for by recording a hologram with a pattern that is distorted in such a way as to produce the desired interconnect pattern at the IR wavelength. This approach typically requires making an intermediate hologram, as described by Aharoni et al. Substantial work in this area has been performed at Stanford University (collimating elements for IR laser diodes) and at the University of Colorado.

The second material issue is associated with scattering noise in photorefractive crystals. Hesselink and Bashaw [38] have recently reviewed the state-of-the-art in holographic data storage, and they show that crosstalk between superimposed holograms is usually much smaller than noise introduced by intrinsic material defects and scattering centers such as striations in SBN. As a result, for successful implementation of a wavelength selectable interconnect pattern, it is necessary that material noise is reduced as much as possible through improved crystal growth techniques or by minimizing the effects of intrinsic scatterers by judiciously choosing the recording geometry.

With respect to improving crystal quality, a great deal of research has been carried out at Stanford University on the growth of small SBN rods using the laser heated pedestal growth technique. Recently, the first a-axis SBN rods have been grown allowing transmission holograms to be recorded. The rod diameter varies from 200-800 microns, which is well suited for the current application.

Using either small rods grown by the laser heated pedestal technique or by carving up a boule of crystalline material into small crystallites as described by Hesselink, an array of elements may be synthesized. With this approach, which is attractive because it minimizes crosstalk between stacks of superimposed interconnect patterns, it is necessary to study the means for fabricating such a

structure. Although a substantial amount of work has been performed on the design and fabrication of such an array for holographic data storage applications, no demonstration array has been fabricated. If a follow-on program is pursued, it is recommended that a demonstration array be fabricated.

6.2 Fixing of Interconnect Patterns

The approach outlined above requires that superimposed holograms must be fixed to avoid erasing every hologram in a stack when one interconnect pattern is addressed. Several approaches have been reported in the literature, including temperature and electrical fixing procedures, as well as achromatic readout in which the wavelength of the readout beam is longer than that of the recording beam. In the latter case the Bragg condition must still be satisfied, which leads to a particular recording and readout geometry, as described by McRuer et al, 1989 [39].

6.3 Previously Reported Fixing Procedures

6.3.1 Temperature Fixing

Thermal fixing schemes are based on writing a hologram using relatively mobile electrons and forming an ionic mirror space charge fields at elevated temperatures where the mobility is sufficiently large to allow the local electric space charge field to establish a corresponding ionic field. The crystal is then cooled to room temperature and illuminated with a uniform readout beam. The electronic space charge field is erased, revealing the ionic field. Because the mobility of ions at room temperature is low, fixing of the hologram over time periods of days is possible. The disadvantage of this approach is the need for heating the crystal, which may introduce distortions in the reconstructed patterns. Temperature fixing has been demonstrated in LiNbO3, and recent work indicates that this may also be possible in SBN (Wilde and Hesselink, 1992) Alternatively, an electrical approach has been reported by Micheron et al. in 1972 [40], but little success has been achieved with this method since then.

6.3.2 Electrical Fixing

The crystal is poled and illuminated with a spatially varying intensity pattern until saturation response is reached. An anti-poling electric field is applied depending on the local space charge field and the coercive field, for typically 1/2 sec. The hologram is then read out by a uniform beam of extraordinary polarization for SBN. The diffracted beam at first decreases in strength, but then grows in amplitude well above the saturation response and maintains that level for several hours. A poling field erases the hologram. This approach has subsequently been demonstrated in other crystals such as LiNbO3; but no published account has been reported for electrical fixing in SBN since this early

effort. Recently, however, progress has been made by Hesselink concerning electrically controlled fixing in SBN:75. Electrically controlled fixing may be achieved by using undoped SBN:75. It is recommended that this research be continued by optimizing the fixing properties of SBN:75 by doping it with Ce and Cr. In addition to studying the fixing properties, erasure and time response issues need to be considered as well.

6.3.3 Crosstalk issues

Crosstalk between superimposed holograms depends on a variety of parameters, including the manner in which the patterns are recorded, the intrinsic scatter noise, and the overlap of Bragg components between patterns. Much work has been reported in the literature on this topic, as summarized by Hesselink and Bashaw in 1993 [38].

Several strategies have been proposed to reduce the effects of crosstalk. A promising approach appears to partition the recording medium into independent regions in which a limited number of holograms are recorded. For example, Hesselink and Redfield [41] have investigated the recording of multiple holograms in small rods of SBN. A large volume of photorefractive material can be synthesized by bundling these photorefractive rods. In each rod, a stack of spatially multiplexed holograms is recorded (Hesselink [42]), and all rods must be optically isolated from each other. The advantages of this approach are:

1) The optical quality of small rods grown with the laser heated pedestal growth method is typically better than for materials grown with the Czochralski technique.
2) The recording regions can be distinct from each other.
3) Larger volumes of material can be synthesized than could be obtained by conventional crystal growing techniques.

In addition, rods of SBN are easier grown than bulk crystals. The rods have dimensions of approximately 0.5 cm in diameter and 3-4 mm in length. Because of the small diameter, the applied field magnitude can be made small (~100 Volts) as well to achieve sufficiently high field values to affect fixing.

To accomplish extensive interconnect capacity, the surface area of the storage medium needs to be large, ultimately approaching 5 x 5 cm. Currently, it is very difficult to grow such large crystals. A mosaic approach needs to be followed to synthesize a medium of sufficient dimensions. The constituents of the mosaic could be smaller bulk crystals or small fiber like rods having a diameter of 0.5 cm with a thickness of a few millimeters long. The cost of implementation is related to the increased complexity of the storage medium. On the other hand, small fibers of SBN tend to be of higher optical quality than bulk crystals which reduces scattering noise effects. Questions related to

the optimum arrangement of the photorefractive microchannel plate should be addressed in greater detail if a follow-on funding is available.

One of the historical drawbacks of using fibers is the orientation of the c-axis; SBN tends to grow preferentially along the c-axis and as a result the fiber and c-axis tend to coincide. Therefore, transmission recording, which produces the strongest index change in SBN when the c-axis is aligned with the grating vector, cannot be achieved in this configuration. Hesselink has recently overcome this problem by growing new SBN fibers in which the c-axis is perpendicular to the fiber axis (a-axis fibers). If it proves to be feasible to grow a-axis fibers of good optical quality, then it is recommended that this approach be utilized to obtain the desired quality.

To implement photorefractive materials as the recording medium for optical interconnect systems, a number of additional materials and fabrication issues need to be resolved. For example, the optimum host material in which the fibers are embedded needs to be determined. In the past Bakelite was used, because it allows ease of fabrication and the hardness approaches that of SBN. Thus, polishing can be effectively carried out without introducing rounded edges on the fiber ends. On the other hand, Bakelite requires a considerable fabrication effort for large arrays, because holes need to be drilled for each rod. Alternatively, epoxies may be used that can be cast around the fiber bundles. In this respect, both electrical and thermal properties of the host material should be considered in fabricating conventional microchannel plates.

6.4 Near Diffraction Limited Performance

To achieve good spatial resolution, the impulse response of the interconnects needs to be made smaller than the required 32x32 micron. This can be achieved by using storage capacity to essentially record more spatial bandwidth than required for the 64K interconnect points/cell. The number of storage bits that are available in a 300x300x3000 micron storage volume is approximately 2.7×10^8, which allows 40 times oversampling of the wavefront, which subsequently gives rise to good diffraction performance.

7.0 Recommendations

7.1 Near Term Objectives

Several device and system level recommendations are suggested for further research if Rome Laboratory chooses to fabricate a multi-channel PROMAC prototype. For example, at the device level, this program has demonstrated that a tunable DBR laser with an internal grating was an incremental component of the PROMAC demonstration model. For the prototype, it is recommended that a TBR laser with electronically tunable sampled gratings be fabricated to

achieve the following performance parameters:

- A tuning range (400 angstroms) sufficient to obtain up to 64 selectable wavelengths (with a wavelength separation of 7 to 10 Å between adjacent wavelengths).
- Wavelength range: 0.8 -1.0 μm.
- Operating wavelength: 9180 Å to 9820 Å.
- Switching time: < 1-10 ns
- Astigmatism: <1 μm
- Collinear, non-steering array output
- Center to center array spacing: 50-250 μm
- Negligible cross-talk
- Near field ≈ 1 x 4 μm
- Mutual incoherence among collinear array lasers
- High spatial and temporal coherence
- Differential quantum efficiency of >30 percent
- Power > 10 mW per element
- Laser material composition: InGaAs/GaAs

The original PROMAC concept at the system level used a tunable laser to illuminate a planar waveguide grating which subsequently illuminated the optical memory. The planar waveguide grating dispersed the incident radiation at an angle proportional to the wavelength (by which it was illuminated). The laboratory prototype demonstrated that by changing the wavelength, angular scanning may be achieved. However, detection through the angular scanning method is limited because the number of bits illuminated in each location of the plate or disk is limited to several hundred to a thousand (bits) at speeds between 1 to 10 ns. Furthermore, tunable lasers are only limited to a few hundred hops An array of lasers could be configured to illuminate a 2D array of 1000 point images, however, the maximum practical memory size would approach approximately 10E8.

The planar wave guide approach or any thin film approach (T < 20 μm), however, does not fulfill the program objectives except for selected applications which include high speed scanning (<1ns/pixel) and low density read only memory access (~4-16k bit). For high density memory systems, efficient selectivity is required.

Volume holographic storage may increase the capacity by 2 to 3 orders of magnitude with read speeds on the order of nanoseconds with DBR tunable lasers. The efficiency of volume holographic storage depends on volume crystal thickness and a reference beam angle (in air) of 60 degrees (θ). A primary objective is to minimize the thickness of the crystal and the reference beam angle. The larger the mode separation on the tunable laser, the better the performance. We believe that a laser can be designed with $\Delta\lambda$ on the order of 10 Å or greater over a 64

nm range centered at 950 nm. This design would reduce the thickness requirement on the crystal is 1 to 3 mm.

The design of this laser will require the most advanced DBR laser technology. To date, a 24 nm bandwidth has been demonstrated. The gain curve of a typical laser diode will support 10% fractional bandwidth. Although 2.5% has been achieved, for the proposed application, ~10% fractional bandwidth is required (which is actually only 6.4%).

To develop an efficient volume holographic optical interconnect element (V-HOIE) design, the following recommendations are suggested:

- Utilize state-of-the-art theoretical models for designing an interconnect element capable of selectively interconnecting 64K points using wavelength control.
- Determine the optimum storage medium from currently available materials.
- Investigate and select suitable fixing techniques.
- Determine the best recording strategy to achieve acceptable performance, i.e. with a sufficiently high signal to noise ratio and spatial resolution.
- Develop a first generation 10x10 element storage medium capable of interconnecting 64, 1000 interconnect planes per element, including a description of required materials properties, recording and readout geometry, and fixing procedures that need to be implemented.

7.2 Long Term Objectives

Ultimately, OptiComp anticipates fabricating fully operational, system level PROMAC devices which will be integrated into current and future high speed, optoelectronic memory systems. It is anticipated that 2D, 64 x 64 PROMAC arrays (4096 elements) will have up to 10E12 interconnects with <1 ns random access. Each PROMAC device will exhibit >1 GHz of bandwidth per channel with 128 tuning frequencies. In addition, the signal-to-noise ratio will average 15 db/bit, power consumption will be approximately 800 aJoules/switch interconnect and cross talk will be minimal. These devices will also have large optical memory address field (> 10 MBytes) and be able to process 1024 x 1024 bits per page. The ultimate storage capacity may be computed as follows:

64 x 64 array	(4096)	
128 tuning frequencies	(128)	
1024 x 1024 bits per page	x (1,048,576)	
	549,755,813,888	bits of information

It is anticipated that PROMAC will be integrated into OptiComp's high performance computing (HPC) module architecture which integrates GaAS DANE technology with "smart' optical interconnects (Figure 31). Through the utilization of PROMAC, it is anticipated that N^5 interconnects will be achievable in the near future.

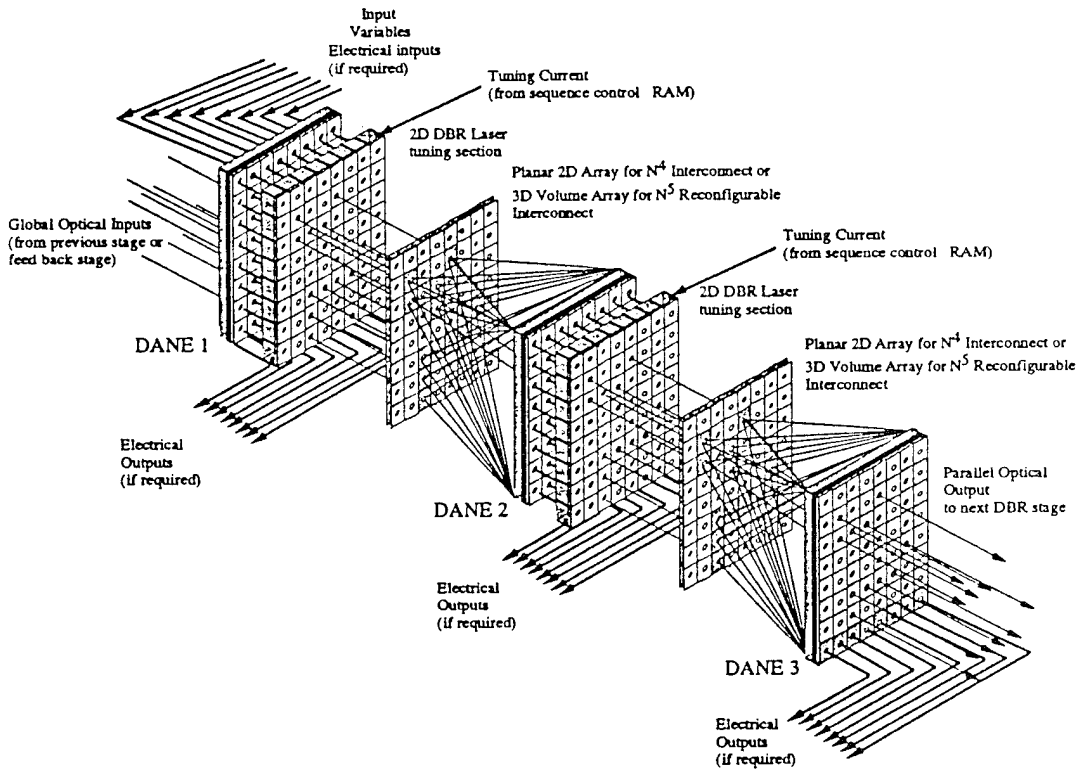

Figure 31: Multi-element, tunable DBR laser with multi-element DANE arrays to achieve reconfigurable N^4 / N^5 global optical interconnects for reprogrammable high performance computing (HPC) modules

Appendix: References

1. "Photonic Random Optical Memory Access Cache", P. S. Guilfoyle, R. V. Stone, Proceedings of the SPIE, Volume 1622-22, February, 1992.
2. The New Physical Optics Notebook: Tutorials in Fourier Optics, Reynolds, DeVelis, Parent and Thompson, Optical Engineering Press, SPIE, Bellingham WA.
3. Optical Holography, Robert Collier, C. Burckhardt and L. Lin, Academic Press, San Diego, CA, 1971.
4. The Photonics Design and Applications Handbook, G.E. Stutz1992.
5. Diffraction Grating Handbook, Milton Roy Corporation, Rochester, NY.
6. "Semiconductor lasers for coherent optical fiber communications", T. L. Koch and U. Koren, J. Lightwave Tech.8, 274-293, March 1990.
7. "The carrier induced index change in AlGaAs and 1.3 μm InGaAsP diode lasers", J. Manning, R. Olshansky and C.B. Su, IEEE J. Quantum Electron. QE-19, 1525-1530, October 1983.
8. "Carrier induced change in refractive index of In, GaAs, and InGaAsP", B.R. Bennett, R.A. Soreff, and J. A. del Alamo, IEEE J. Quantum Electron. 26, 113-121, Jan. 1990.
9. "Tunable diode laser design for communication and ranging", J M Hammer, Monthly reports # 1, Nov.'91; #2, Dec.'91; #5 March'92; and 6, April 1992, NASA Contract Number NAS1-19000, Contract # 17GFY910412.
10. Monthly Report April 1992 Prepared for David Sarnoff Research Center.
11. "Continously - Tunable Single Frequency Semiconductor Lasers", Coldren and S.W. Corzine, IEEE Journal of Quantum Electronics, Vol. QE 234, No. 6, June 1987.
12. "Over 7 nm (875) GHz) continuous wavelength tuning by tunable twin-guide (TTG) laser diode", Illek, S.; Thulke, W.; Schanen, C.; Lang, H.; Amann, M.-C., Electron Lett. 26. (#1), 46-47, 4 Jan. 1990.
13. "Continuously tunable single-frequency laser diode utilizing transverse tuning scheme", Amann, M.-C.; Illek, S.; Schanen, C.; Thulke, W.; Lang, H., Electron Lett. 25, 837-9, 22 June 1989.
14. "Tunable twin-guide laser: a novel laser diode with improved tuning performance", Amann, M.-C.; Illek, S.; Schanen, C.; Thulke, W., Applied Physics Lett.,54, .2532-3 19 June 1989.
15. "Wavelength tuning characteristics of tunable twin-guide lasers with improved current-injection structures", E Yamamoto et al,Appl. Phys. Lett. 60,805, 17 Feb. 1992
16. "Grating-assisted InGaAsP/InP vertical codirectional coupler filter", R.C. Alferness et al, Appl. Phys. Lett., 55, 2011 Nov. 1989
17. "Directional couplers made of nonidentical assymetric slabs. Part II: Grating-assisted coupler", D. Marcuse, J. Lightwave Tech., LT-5, 268 Feb. 1987.
18. "Frequency response and tunability of grating-assisted directional couplers", G. Griffel and A. Yariv, J. Quant. Electron., 27, 1115, May 1991.
19. "InGaAsP/InP buried rib waveguide vertical coupler filter", R.C. Alferness et al, Opt. Fiber Conf., San Diego CA, 1991, Paper ThB2.

20. "Monolithic tunable semiconductor laser using a mismatched-waveguide directional-coupler filter", Z.M. Chuang and L.A. Coldren, IEEE-LEOS Ann. Meet.San Jose, CA, 1991.

21. "Wavelength tuning in a grating-assisted vertical coupler filter using quantum well electrorefraction", H. Sakata, S Takeuchi, Appl. Phys. Lett. 59,3081, 9 Dec. 1991.

22. "Strained inGaAS/GaAs quantum well constricted-mesa lasers and application in avertical-twin-guide tunable laser", Z. M. Chuang , et al, Photon Tech. Lett., 4, 315, April 1992.

23. "Codirectionally coupled twin-guide laser diode for broadband electronic wavelength tuning", Illek, S.; Thulke, W.; Amann, M.-C., Electron. Lett, 27,.2207-9, 21 Nov. 1991.

23a "Low Threshold, High Power, Vertical Cavity Surface Emitting Lasers,"R.S. Geels and L.A. Coldren, *Electronics Letters*, vol. 27, No. 21, pp. 1984-1985, Oct. 10, 1991.

23b "Three-terminal vertical cavity laser diodes for wavelength tuning and stabilization,"T. Wipiejewski, K. Panzlaff, E. Zeeb, and K. J. Ebeling, submitted to OFC '93.

23c "High-Power Temperature-Insensitive, Gain-Offset InGaAs/GaAs Vertical-Cavity Surface-Emitting lasers,"D.B. Young, J.W. Scott, F.H. Peters, B.J. Thibeault, S.W. Corzine, M.G. Peters, S.L.Lee, and L.A.Coldren, to be published in *IEEE Photonics Letters,* Feb. '93.

24. "Demonstration of broadband tunability in a semiconductor laser using sampled gratings", VJayaraman, D.A.Cohen and L.A. Coldren, Appl. Phys. Lett., 60, 2321-2323, 11 May 1992.

24a "Very wide tuning range in a sampled grating DBR laser", V. Jayaraman, A. Mather, L.A. Coldren, P.D. Dapkus, 13th International Semiconductor Laser conference, post- deadline paper, Takamatsu, Kagawa, Japan, 1992.

25. "The optical gain lever; a novel gain mechanism in the direct modulation of quantum well semiconductor lasers", K.J. Vahala, M.A. Newkirk and T.R. Chen, Appl.Phys Lett., 54, 2506-2508, 19 June 1989.

26. "Ultrahigh efficiency microwave signal transmission using tandem-contact single quantum well GaAlAs lasers", N. Moore and K. Y. Lau, Appl.Phys Lett., 55, 936-938, Sept. 1989.

27. "Intensity noise in the ultrahigh efficiency tandem-contact quantum well lasers", D. Gajic and K. Y. Lau, Appl.Phys Lett., 57, 1837-1839, 29 Oct. 1990.

28. "Frequency modulation and linewidth of gain-levered two-section single quantum well lasers", K. Y. Lau, Appl.Phys Lett., 57, 2068-2070, 12 Nov. 1990.

29. "Broad wavelength tunability in gain-levered quantum well semiconductor lasers", K. Y. Lau, Appl.Phys Lett., 57, 2632-2634 , 17 Dec. 1990.

30. "Narrow linewidth continuously tunable semiconductor lasers based on quantum well gain lever", K. Y. Lau, Appl.Phys. Lett., 59, 2216-2218, 28 Oct . 1991.

31. "Comparison of vertically-compact high-speed GaAs and $In_{0.35}Ga_{0.65}As$ MQW Diode Lasers Designed for Monolithic Integration", J. D. Ralston et al., 13th IEEE International Semiconductor Laser Conference Digest, 176-177, 21-25 Sept. 1992.

32. "Broadband tunability of gain-flattened quantum well semiconductor lasers with an external grating", M. Mittelstein et al., Appl.Phys Lett., 54, 1092-1094 , 20 Mar. 1989.
33. "$Ga_{0.8}In_{0.2}As/GaAs/Ga_{0.51}In_{0.49}P$ buried ridge structure single quantum well laser emitting at 0.98 μm", K. Mobarhan et al., Electron. Lett., 28, 1510-1511 , 30 Jul. 1992.
34. "Ultralow threshold strained InGaAs-GaAs quantum well lasers by impurity-induced disordering", W. X. Zou et al., Electron. Lett., 27, 1241-1243 , 4 Jul. 1991.
35. "Demonstration of a monolithic, grating-surface-emitting laser master oscillator-cascaded power amplifier array", N. W. Carlson et al., Photon. Technol. Lett., 2, 708-710, Oct. 1990.
36. "Microchannel Heat Sinks for Two-Dimensional High-Power-Density Diode Laser Arrays", L. J Missaggia et al., J. Quant. Electron., 25, 1988, 1989.
37. "Modular microchannel cooled heatsinks for high average power laser diode arrays", Beach et al., J. Quant. Electron., 28, 966-976, Apr 1992.
38. "Optical memories implemented with photorefractive media", Hesselink, L and Bashaw, M.C., invited paper to be published in Spring of 1993 in Journal of Optics and Electronics.
39. "Two wavelength photorefractive dynamic optical interconnect", McRuer, R, Wilde, J, Hesselink, L and Goodman, J, 1989, Opt. Lett., 14 (21), 1174.
40. "Electrical control of fixation and erasure of holographic patterns in ferroelectric materials", Micheron, F and Bismuth, G 1972, , Appl. Phys. Lett, 32 (3).
41. "Photorefractive holographic recording in strontium niobate fibers", Hesselink, L and Redfield, S, 1988,, Opt. Lett. 13 (10), 877.
42. "Photorefractive fibers for optical data storage and processing", Hesselink, L, 1990, , Int J. of Optoelect., 5 (2), 103.

MISSION

OF

ROME LABORATORY

Mission. The mission of Rome Laboratory is to advance the science and technologies of command, control, communications and intelligence and to transition them into systems to meet customer needs. To achieve this, Rome Lab:

a. Conducts vigorous research, development and test programs in all applicable technologies;

b. Transitions technology to current and future systems to improve operational capability, readiness, and supportability;

c. Provides a full range of technical support to Air Force Materiel Command product centers and other Air Force organizations;

d. Promotes transfer of technology to the private sector;

e. Maintains leading edge technological expertise in the areas of surveillance, communications, command and control, intelligence, reliability science, electro-magnetic technology, photonics, signal processing, and computational science.

The thrust areas of technical competence include: Surveillance, Communications, Command and Control, Intelligence, Signal Processing, Computer Science and Technology, Electromagnetic Technology, Photonics and Reliability Sciences.